Airway epithelial responses to rhinovirus, coronavirus and cigarette smoke

Wang, Y.

Chapter 5

Impact of changes in human airway epithelial cellular composition and differentiation on SARS-CoV-2 infection biology

Ying Wang,[a*] Melissa Thaler,[b*] Anne M. van der Does,[a] Alen Faiz,[c] Dennis K. Ninaber,[a] Natacha S. Ogando,[b] Hendrik Beckert,[d] Christian Taube,[d] Clarisse Salgado-Benvindo,[b] Eric J. Snijder,[b] Peter J. Bredenbeek,[b] Pieter S. Hiemstra,[a#] Martijn J. van Hemert[b#]

[a]Department of Pulmonology, Leiden University Medical Center, Leiden, the Netherlands.

[b]Department of Medical Microbiology, Leiden University Medical Center, Leiden, the Netherlands.

[c]University of Technology Sydney, Respiratory Bioinformatics and Molecular Biology (RBMB), School of Life Sciences, Sydney, Australia.

[d]Department of Pulmonary Medicine, University Medical Center Essen – Ruhrlandklinik, Essen, Germany

*These authors share first authorship

[#]These authors contributed equally to this work

Published as pre-print on bioRxiv 2021: doi: 10.1101/2021.07.21.453304
submitted to peer-reviewed journal

Abstract

The consequences of infection with severe acute respiratory syndrome coronavirus 2 (SARS-CoV-2) can range from asymptomatic to fatal disease. Variations in epithelial susceptibility to SARS-CoV-2 infection depend on the anatomical location from the proximal to distal respiratory tract. However, the cellular biology underlying these variations is not completely understood. Thus, air-liquid interface (ALI) cultures of well-differentiated primary human tracheal and bronchial epithelial cells were employed to study the impact of epithelial cellular composition and differentiation on SARS-CoV-2 infection by transcriptional (RNA sequencing) and immunofluorescent analyses. Changes of cellular composition were investigated by varying time of differentiation or by using specific compounds. We found that SARS-CoV-2 primarily infected ciliated cells but also goblet cells and transient secretory cells. Viral replication was impacted by differences in cellular composition which depended on culturing time and anatomical origin. A higher percentage of ciliated cells correlated with a higher viral load. However, DAPT-treatment, which increased number of ciliated cells and reduced goblet cells, decreased viral load, indicating the contribution of goblet cells to infection. Cell-entry factors, especially cathepsin L and transmembrane protease serine 2, were also affected by differentiation time. In conclusion, our study demonstrates that viral replication is affected by changes in cellular composition, especially in cells related to the mucociliary system. This could explain in part the variable susceptibility to SARS-CoV-2 infection between individuals and between anatomical locations in the respiratory tract.

Introduction

Since December 2019, severe acute respiratory syndrome coronavirus 2 (SARS-CoV-2) has rapidly spread worldwide. The burden of the associated coronavirus disease 2019 (COVID-19) has an enormous medical, social and economic impact (1). Furthermore, the continuing emergence of virus variants, such as the delta and omicron variants, are associated with additional waves of COVID-19 cases (2, 3). This illustrates the threat of these viruses to prolong the current pandemic or lead to new large outbreaks in the future. Besides different clinical outcomes due to SARS-CoV-2 variants, even people infected with the same virus variant present with varying clinical signs and symptoms depending on age (4), sex (5), weight (6), environment (7), other medical conditions (6, 8), immune status (9), and possibly other yet to be identified factors.

SARS-CoV-2 was first isolated from the lower respiratory tract of COVID-19 patients (10, 11). The epithelium serves as the first barrier to SARS-CoV-2 infection in the respiratory tract and therefore the subsequent epithelial response to infection (antiviral and inflammatory responses) plays an important role in the outcome of infection. The respiratory tract spans from the nasal cavity to the terminal bronchioles, ending in the alveoli where gas exchange occurs. The airways are lined by the airway epithelium, which includes various cell types, of which ciliated, secretory goblet and club cells, and basal cells are present in the highest numbers (12, 13). These cell types have their own distinct functions. For instance, goblet cells secrete mucus, which captures inhaled particles like respiratory viruses, while the continuous beating cilia from ciliated cells help to transport this mucus with entrapped particles towards the pharynx, collectively called mucociliary clearance (MCC). Although the airway epithelium shares similar cell types throughout the respiratory tract, the proportion of each cell type is dependent on the anatomical location (14). In addition, in many patients with lung diseases such as asthma or chronic obstructive pulmonary disease (COPD), epithelial cellular composition is altered (13). In primary airway epithelial cell cultures, which are differentiated at the air-liquid interface (ALI), cellular composition of the airway epithelium depends on the individual donor (15), differentiation time (16), and culture conditions (17). So far, the impact of epithelial cellular composition on SARS-CoV-2 infection biology has not been completely elucidated. Previous studies have demonstrated a difference in host susceptibility to SARS-CoV-2 infection depending on the location of virus-host interaction in the respiratory tract (18). However, it is unclear to what extent the differences in viral replication link to variation in epithelial cellular composition. SARS-CoV-2 targets ciliated and secretory cells (19, 20), possibly via strands of mucus attached to cilia tips (21). Therefore, changes in the proportion of these target cells might affect viral replication. SARS-CoV-2 cellular tropism furthermore depends on host proteins that are involved in virus entry, including angiotensin converting enzyme 2 (ACE2) and proteases like transmembrane protease serine 2 (TMPRSS2)

and cathepsin L (CTSL), as well as alternative receptors (e.g. cluster of differentiation 147 [CD147], 78-kDa glucose-regulated protein [GRP78], tyrosine-protein kinase receptor UFO [AXL]), which all have been demonstrated to be expressed in variable levels on human airway epithelial cells (22-25). Recent research demonstrated that SARS-CoV-2 cell-entry factors are primarily expressed in bronchial transient secretory cells (26), indicating these transiently differentiating cells might contribute to a great extent to initial infection.

While research on the susceptibility of respiratory epithelial cells to SARS-CoV-2 infection often focuses on a specific cell-type, function or protein of interest (27), we aimed to investigate how various changes in cellular differentiation and composition affect SARS-CoV-2 infection biology. This knowledge can support our understanding of how these factors could contribute to local, and - more importantly - airway disease-associated differences in susceptibility. To this end, we used primary human bronchial (PBEC) and tracheal epithelial cells (PTEC) and differentiated them at the air-liquid interface (ALI) for up to 5 weeks. We characterized virus replication, spread, localization, immune responses, and expression of SARS-CoV-2-entry factors, as well as compared cellular composition between both types of cultures. Furthermore, we investigated how infection characteristics were influenced by modulation of the cellular composition and by the duration of culture.

Materials and Methods

Cell culture

PBEC were isolated from tumor-free resected bronchial tissue that was obtained from patients undergoing resection surgery for lung cancer at the Leiden University Medical Center (Leiden, the Netherlands). Patients from which this PBEC were derived were enrolled in the biobank via a no-objection system for coded anonymous further use of such tissue (www.coreon.org). However, since 29-11-2020, patients have been enrolled in the biobank using active informed consent in accordance with local regulations from the LUMC biobank with approval by the institutional medical ethical committee (B20.042/Ab/ab and B20.042/Kb/kb). PTEC were isolated from residual tracheal and main stem bronchial tissue from lung transplant donors post-mortem at the University Medical Center Essen (Essen, Germany). Use of such donor tissue for research was approved by the ethical committee of the Medical faculty of the University Duisburg-Essen (ID: 19-8717-BO). After isolation, cells were expanded in T75 flasks and frozen in liquid nitrogen until use as previously described (28).

To achieve mucociliary differentiation, PBEC and PTEC were cultured at the ALI as previously described (29). Briefly, epithelial cell cultures from individual donors or mixed donors were seeded onto 12-insert Transwell membranes (Corning Costar,

Cambridge, MA, USA), which were coated with PBS supplemented with 5 µg/ml human fibronectin (Promocell, Heidelberg, Germany), 30 µg/ml PureCol (Advanced BioMatrix, CA, USA) and 10 µg/ml bovine serum albumin (Fraction V; Thermo Fisher Scientific, Carlsbad, CA, USA), in a 1:1 mixture of Bronchial Epithelial Cell Medium-basal (BEpiCM-b; ScienCell, Sanbio) and Dulbecco's modified Eagle's medium (DMEM) (Stemcell Technologies, Köln, Germany), further referred to as B/D medium. This B/D medium contains 12.5 mM HEPES, bronchial epithelial cell growth supplement, 100 U/ml penicillin, 100 ug/ml streptomycin (all from ScienCell), 2 mM glutaMAX (Thermo Fisher Scientific). B/D medium was supplemented during submerged culture with 1 nM EC23 (light-stable retinoic acid receptor agonist; Tocris, Abingdon, UK). For individual donors, the seeding intensity was 40,000 cells/12-insert and for mixed donors approximately 150,000 cells (30,000 cells/donor when mixing cells from 5 donors and 40,000 cells/donor when using 4 donors). For the donor mixes, the higher seeding density compared to individual cultures resulted in near-confluency to avoid selective advantage of possible faster-proliferating cells of specific donors.

After confluency was reached, the apical medium was removed and cells were cultured at the ALI in B/D medium with 50 nM EC23 for 3-5 weeks; during this period, medium was refreshed and the apical side was washed three times a week with warm PBS to remove excess mucus.

To shift cell differentiation towards an increased number of goblet or ciliated cells, ALI- PBEC were incubated in BD medium supplemented with 50 nM EC23, and either 1 ng/ml IL-13 (Peprotech) or 5 µM DAPT (γ-secretase inhibitor, TOCRIS) from day 22 to day 35 culture time. To assess the direct effect of DAPT, we treated cells with DAPT either starting 24 h before (and during) infection (a time period considered insufficient to cause a shift in epithelial differentiation) or directly after infection.

Vero E6 cells (master stock MM-3 from dept. of Medical Microbiology collection, characterized by full genome sequencing) were maintained in Dulbecco's modified Eagle's medium with 4.5 g/l glucose with L-glutamine (DMEM; Lonza), supplemented with 8% foetal calf serum (FBS; CapriCorn Scientific) and 100 U/ml of penicillin/streptomycin (Sigma-Aldrich). All cell cultures were maintained at 37°C. Infections for plaque assays in Vero E6 cells were performed in Eagle's minimal essential medium with 25 mM HEPES (EMEM; Lonza) supplemented with 2% FCS, 2 mM L-glutamine (Sigma-Aldrich), and 100 U/ml of penicillin/streptomycin (Sigma-Aldrich) .

SARS-CoV-2 virus

The clinical isolate SARS-CoV-2/Leiden-0002 was isolated from a nasopharyngeal sample collected at the LUMC (GenBank accession nr. MT510999). The virus was

passaged twice in Vero E6 cells to obtain the virus stock used for infection. Virus titers were determined by plaque assay as described before (30). All experiments with infectious SARS-CoV-2 were performed at the Leiden University Medical Center biosafety level 3 facilities.

SARS-CoV-2 infection of ALI-PBEC

Prior to infection, the mucus was removed by washing the apical surface of the ALI cultures with 200 µl PBS and aspirating it after a 10-min incubation at 37°C. Basal medium was changed every two days. Cells were infected with 200 µl of inoculum prepared in PBS, containing 30,000 PFU of SARS-CoV-2, per insert for 2 h at 37°C on a rocking platform (estimated MOI of 0.03). PBS was used as a solvent control and in mock-infected cells as inoculum. After removal of the inoculum, the apical side was washed three times with PBS and cells were incubated at 37°C. Viral progeny was harvested from the apical side at 24, 48 and 72 hpi as described in the next section.

Cells were infected after 3 to 5 weeks of differentiation as indicated. For cells under DAPT or IL-13 treatment, the medium was supplemented with 1 ng/ml IL-13 or 5 µM DAPT after 3 weeks of differentiation, and after 5-week culture time in total (2 weeks of treatment), PBEC were infected. After infection, the basal medium was replaced by fresh B/D medium also supplemented with IL-13 or DAPT.

RNA isolation, quantitative RT-PCR/real-time PCR (RT-qPCR) and plaque assay analysis

Apical washes were harvested following a 10-min incubation at 37°C with 200 µl. RNA was isolated from half the volume of apical washes (100 µl) after addition of 800 ul of TriPure Isolation Reagent (Sigma-Aldrich). Tripure reagent was spiked with Equine arteritis virus (EAV) to control for variation in RNA extraction efficiency and possible inhibitors of RT-qPCR. Intracellular RNA was isolated by adding 500 ul of TriPure reagent directly to cells onto the insert. Samples were stored at -20°C until RNA was isolated using the Direct-zol™ -96 RNA plate isolation (Zymo), 5PRIME Phase Lock Gel extraction (Quantabio) or Maxwell® 16 simply RNA tissue kit (Promega, the Netherlands). The Phosphoglycerate kinase 1 (*PGK-1*) was used as a reference gene for normalization when intracellular RNA was analysed. Primers and probes for EAV and *PGK-1* (Sigma-Aldrich) and the normalization procedure were performed as described before(30). Viral RNA was quantified by internally controlled multiplex RT-qPCR using the TaqMan™ Fast Virus 1-Step Master Mix (Thermo Fisher Scientific) as described previously (31), but with modifications as listed in Table 1. A standard curve generated by RT-qPCR on 10-fold serial dilutions of a T7 RNA polymerase-generated *in vitro* transcript containing the target sequences was used for absolute quantification of RNA copy numbers.

Table 1 Primer sequences

Gene	Forward primer (5'-3')	Reverse primer (5'-3')
E	ACAGGTACGTTAATAGTTAATAGCGT	ATATTGCAGCAGTACGCACACA
E probe	TexRed-ACACTAGCCATCCTTACTGCGCTTCG-BHQ1	
RdRp	GTGARATGGTCATGTGTGGCGG	CARATGTTAAASACACTATTAGCATA
RdRp probe	FAM-CAGGTGGAACCTCATCAGGAGATGC-BHQ1	
MUC5AC	CCTTCGACGGACAGAGCTAC	TCTCGGTGACAACACGAAAG
FOXJ1	GGAGGGGACGTAAATCCCTA	TTGGTCCCAGTAGTTCCAGC
SCGB1A1	ACATGAGGGAGGCAGGGGCTC	ACTCAAAGCATGGCAGCGGCA
TP63	CCACCTGGACGTATTCCACTG	TCGAATCAAATGACTAGGAGGGG
IFNL1	GGACGCCTTGGAAGAGTCACT	AGAAGCCTCAGGTCCCAATTC
IFNB1	ATGACCAACAAGTGTCTCCTCC	GGAATCCAAGCAAGTTGTAGCTC
CXCL8	CTGGACCCCAAGGAAAAC	TGGCAACCCTACAACAGAC
IL6	CAGAGCTGTGCAGATGAGTAC A	GATGAGTTGTCATGTCCTGCA
ACE2	CGTCTGAATGACAACAGCCTAGA	AATGCCAACCACTATCACTCCC
TMPRSS2	AATCGGTGTGTTCGCCTCTAC	CGTAGTTCTCGTTCCAGTCGT
CD147	CAGAGTGAAGGCTGTGAAGTCG	TGCGAGGAACTCACGAAGAAC
GRP78	GGAAAGAAGGTTACCCATGC	AGAAGAGACACATCGAAGGT
ATP5B	TCACCCAGGCTGGTTCAGA	AGTGGCCAGGGTAGGCTGAT
RPL13A	AAGGTGGTGGTCGTACGCTGTG	CGGGAAGGGTTGGTGTTCATCC

For analysis of the transcriptional response of epithelial cells to infection, RNA was reverse-transcribed and cDNA was amplified by real-time qPCR (Bio-Rad, Veenendaal, the Netherlands) using specific primers. Relative normalized gene expression compared to reference genes Ribosomal Protein L13a (RPL13A) and ATP synthase, H^+ transporting, mitochondrial F1 complex, beta polypeptide (ATP5B) were calculated according to the standard curve method. Reference genes were selected out of 8 candidate reference genes using the "Genorm" software (Genorm; Primer Design, Southampton, UK). RT-qPCR was performed on a CFX384 Touch™ Real-Time PCR Detection System (Bio-Rad) using a program consisting of 5 min at 50°C and 20 s at 95°C (or 3 min at 95°C when cDNA was used), followed by 45 cycles of 5 s at 95°C and 30 s at 60°C or 63°C (depending on primers).Primer pairs are listed in Table 1.

For quantification of the number of infectious virus particles, the apical wash was serially diluted and infectious titers were determined by plaque assay on Vero E6 as described previously (30).

Immunofluorescence staining

For analysis by immunofluorescence, ALI cultures were rinsed using PBS and cells

were fixed by adding 3% (w/v) paraformaldehyde diluted in PBS into the basal and apical compartments followed by incubation at room temperature for at least 35 min. Next, inserts were washed two times with PBS and stored in PBS with 10 mM glycine at 4°C until further use. Ice-cold methanol was added for 10 min at 4°C, and PBS containing 1% (w/v) BSA, 0.3% (w/v) Triton-X-100 (PBT) was used to block non-specific binding sites and permeabilize cells for 30 min at 4°C. Membranes were excised from the insert and cut into 4 pieces that were incubated overnight at 4oC with specific antibodies at the following dilutions: rabbit anti-SARS-CoV-2 N antibody (JUC3,1:500 (32)), human anti-SARS-CoV-2 Spike antibody (P008_076 (33)), mouse anti-MUC5AC antibody (1:200; Thermo Fisher Scientific), mouse anti-acetylated α-tubulin (1/100; Sigma Aldrich) or goat anti-FOXJ1 antibody (1:200; R&D, Minneapolis, MN, USA). After washing, membranes were incubated with corresponding secondary antibodies: donkey anti-rabbit, donkey anti-mouse or donkey anti-goat Alexa-fluor antibodies (all diluted 1:200, Thermo Fisher Scientific) and 4',6-diamidino-2-phenylindole (DAPI, 1:200, Sigma-Aldrich) in the dark for 30 min at room temperature. Next, membranes were transferred to glass slides and covered with prolong gold anti-fading reagent (Thermo Fisher Scientific) and a coverslip (VWR, Amsterdam, the Netherlands). Slides were viewed using a Leica TCS SP8 confocal microscope (Leica Microsystems, Wetzlar, Germany) at 100 x /400 x / 630 x original magnification according to experimental requirements or ZEISS Axio Scan.Z1 Slide Scanner (ZEISS, Oberkochen, Germany). Positive-stained cells from three random areas of each insert membrane of each independent experiment were quantified by ImageJ.

RNA sequencing and analysis

The samples harvested from 3-week and 5-week differentiated ALI-PBEC and ALI-PTEC were used to perform RNA sequencing (RNA-Seq) at GenomeScan (Leiden, the Netherlands). Total RNA was extracted using TriPure Isolation Reagent and Maxwell® 16 simply RNA tissue kit and passed the quality control (QC) measured by the Fragment Analyzer. Then mRNA was isolated based on poly-A selection and further performed RNA fragmentation. After that, cDNA was synthesized for adapter ligation and PCR amplification. A data set of 12 samples was generated using an Illumina NovaSeq6000 sequencer and the quality for the raw data was determined with third-party (FastQC v0.11.9) and in-house (FastQA v3.1.25) QC tools. The paired-end reads were trimmed to remove possible adapter sequences using cutadapt v2.10 and mapped to the human GRCh37.75 (Homo_sapiens.GRCh37.75.dna.primary assembly.fa). Based on the mapped locations in the alignment file the frequency of how often a read was mapped on a transcript was determined with HTSeq v0.11.0. RNA-Seq analysis was performed using the R package DeSeq2 with the read counts≥10 read counts. Differential expression was conducted comparing virus infection at each time point to time matched no virus control/mock. Gene signatures were made using the Gene Set Variation Analysis (GSVA) package.

The differentially expressed genes (DEGs) were generated by comparing data in 5-week cultures compared to 3-week cultures and the significant differences were considered when they had a Benjamini Hochberg p value<0.1 and a fold change>|2|. The gene sets of differentially expressed genes were further analysed by gene set enrichment analysis (GSEA) using the website www.gsea-msigdb.org as previously reported (34, 35).

Cellular deconvolution

The relative proportion of each cell type (ciliated, secretory, basal and rare cells) was predicted using cellular deconvolution analysis of bulk RNA-Seq data as previously described (36). To this end, genes were selected using AutoGeneS software on the Human Lung Cell Atlas v1.0 dataset (37) based on minimized correlation and maximized distance between clusters. After that, genes with the most stable results across cohorts were selected and used to deduce major cell type proportions. The RNA-Seq data was subsequently normalized to counts per million (CPM), and highly variable (HV) genes (N=5,000) were selected. Next, on all samples bulk deconvolution was performed using the CIBERSORT support vector regression (SVR) method (38). The relative proportion of cell types was compared between 3-week cultures and 5-week cultures from ALI-PBEC or ALI-PTEC using paired two-way ANOVA with Tukey's test.

Statistical analysis

Statistical analysis was performed in GraphPad PRISM 9.0 (GraphPad Software Inc., La Jolla, CA). Differences were assessed by a paired one-way with Tukey's test, paired two-way ANOVA with Tukey's test or paired, two-tailed t test. Data are shown as mean values ± SEM and differences were considered significant at $P < 0.05$.

Results

Susceptibility of airway epithelial cultures to SARS-CoV-2 differs between individual donors

To investigate the effect of differentiation status and cellular composition of the airway epithelium on SARS-CoV-2 infection biology, we first aimed to establish a reliable infection model. We investigated donor-dependent variability in infection by comparing SARS-CoV-2 replication kinetics in cultures of 4 individual donors and a mix of those donors. Between the single donor cultures, we observed some variation in viral load (Fig. 1a). Cultures derived from mixes of primary cells from these donors (donor mix) showed comparable infection kinetics with regard to this variation, and immunofluorescence staining confirmed similar numbers of infected cells at 72 hours post infection (hpi) for single donors and donor mix (Fig. 1b). Thus ALI-PBEC cultures of mixed donor cells proved to be a representative model to

investigate characteristics of airway epithelial cell cultures and test many variables to, while keeping sample size relatively limited.

We performed infections at a relatively low multiplicity of infection (MOI) to model the initial stage of infection by initially only infecting a fraction of susceptible cells and observe the virus spread across the epithelium over time. Four independent experiments were performed using ALI-PBEC derived from the same donor mix. After infection with SARS-CoV-2 (estimated 30,000 PFU per insert), we observed an increase in viral load (extracellular copies of viral RNA) over time, to approximately 10^{11} copies/ml at 72 hpi (Fig. 1c). Immunofluorescence staining of the epithelial cultures for viral nucleocapsid protein also showed a gradual increase in the number of infected cells over time (Fig. 1d). The number of infected cells was low and generally detected at the edge of the insert (Fig. S1a) as also previously reported (39).

To validate the relevance of our cell culture model for studying epithelial defence against SARS-CoV-2 infection, we measured antiviral responses (IFN-β1 and IFN-λ1) and inflammatory cytokines (IL-6 and IL-8 [CXCL8]) (Fig. S1). We observed that SARS-CoV-2 infection did not affect mRNA levels of *IFNB1* and *IFNL1* at 24 and 48 h, but strongly increased their expression at 72 hpi (Fig. S1b). At 72 hpi, mRNA levels of both *IL6* and *CXCL8* displayed a modest but significant increase in SARS-CoV-2-infected cultures (Fig. S1c). We established reproducible and robust infection kinetics in this model, accompanied by a significant but late epithelial antiviral and inflammatory response that is characteristic for SARS-CoV-2 infection (40).

SARS-CoV-2 primarily infects epithelial cells involved in mucociliary clearance

Previous studies have indicated that within the human respiratory tract, predominantly ciliated cells, but also goblet cells of the airway epithelium can be infected with SARS-CoV-2 (19), as well as alveolar epithelial cells (41, 42). To assess if ciliated and goblet cells were also the target cells in our cultures, we investigated the colocalization of SARS-CoV-2 nucleocapsid protein with either acetylated α-tubulin and FOXJ1 as markers for ciliated cells, or MUC5AC as a marker for goblet cells. Recently, a new transient secretory cell subtype which is positive for markers of ciliated and goblet cells, was suggested to be particularly susceptible to SARS-CoV-2 based on ACE2 and TMPRSS2 expression (43). We observed presence of most of the viral nucleocapsid protein in acetylated α-tubulin-positive ciliated cells in ALI-PBEC cultures, with less presence in $MUC5AC^+$ goblet cells (Fig. 1e), showing that both cell types can indeed be infected by SARS-CoV-2. Additionally, immunofluorescence staining showed that few transient secretory cells - defined as FOXJ1 and MUC5AC double-positive cells - were present and infected by SARS-CoV-2 (Fig. 1f).

We next investigated if the number of SARS-CoV-2 target cells in the single donor cultures depicted in Fig. 1a, correlated with the level of infection. Interestingly, quantification by immunofluorescence staining showed that cultures from donor 3, which had the higher initial viral load (at 24 hpi) compared to cells from donor 1 with the lowest initial viral load, constituted a higher proportion of FOXJ1^{+} ciliated cells, as well as transient secretory cells (Fig. 1g). This result suggests that the differences in susceptibility of cultures from different donors to viral infection might be associated with variation in the percentages of the different SARS-CoV-2 target cells.

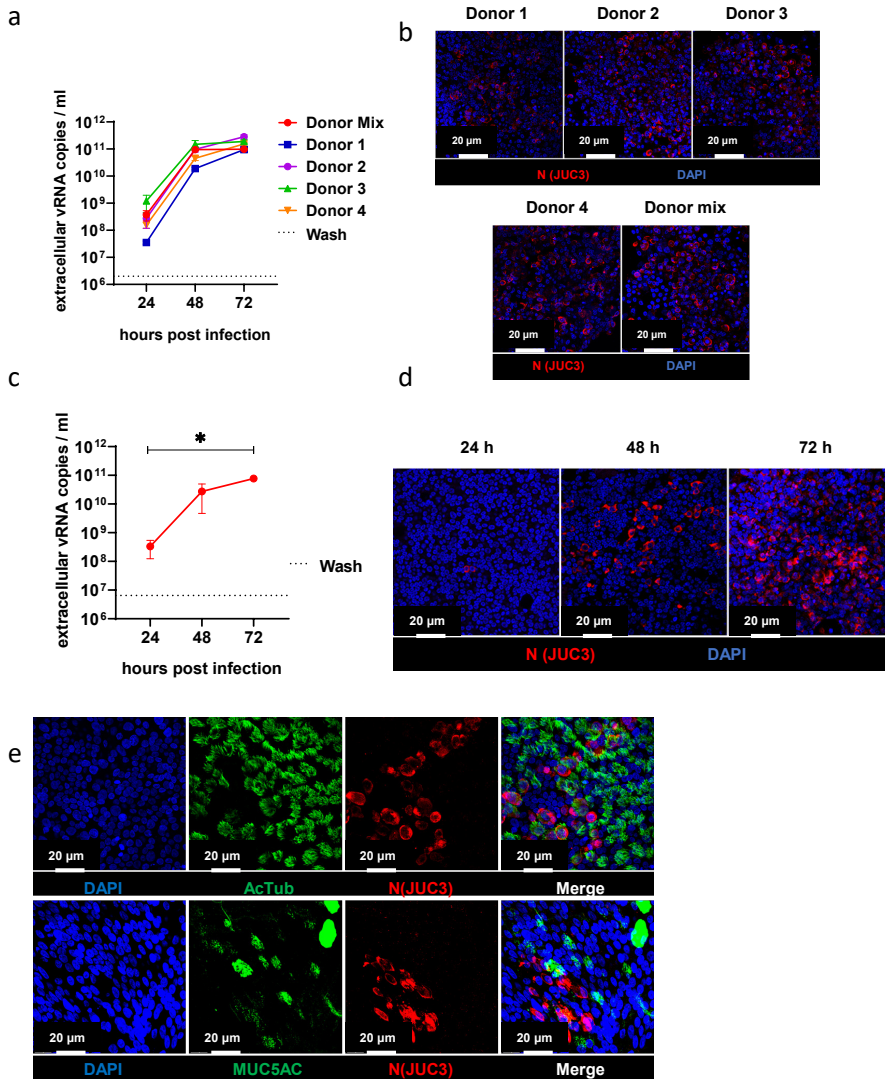

Continued to next page

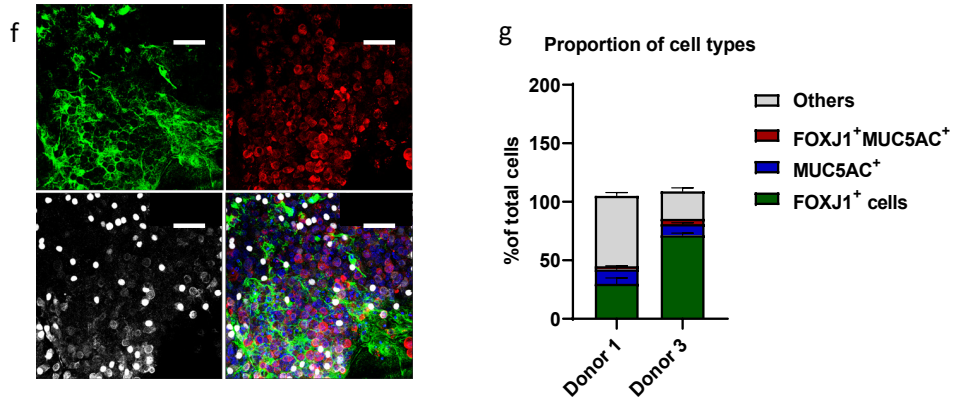

Figure 1. Characterization of a SARS-CoV-2 infection model using air-liquid interface cultures of primary bronchial epithelial cells. Mixes of PBEC derived from 4-5 individual donors were cultured for 5 weeks at ALI before they were infected with SARS-CoV-2 (30,000 PFU per insert). (a) The viral load in cultures derived from single donors or a mix of these donors (in red) was determined by quantifying the level of extracellular viral RNA copies by RT-qPCR. The dashed line represents the amount of (input) viral RNA that remained in the last wash after washing the inserts at 2 hpi (mean of all donors). (b) The infected cells were stained with rabbit polyclonal anti-SARS-CoV-2 N protein antibody (JUC3) and with 4',6-diamidino-2-phenylindole (DAPI), and visualized by immunofluorescence microscopy at 72 hpi. Images shown at 400 x original magnification are representative for results obtained with cells from random areas of the inserts. (c) The viral load at 24, 48 and 72 hpi in cultures was determined by quantifying the number of extracellular viral RNA copies by RT-qPCR. Data are mean ± SEM. n=4 independent experiments with the same donor mix. (d) For immunofluorescence microscopy, cells were fixed at 72 hpi and (double) labelled with rabbit polyclonal anti-SARS-CoV-2 N protein antibody (JUC3) and with DAPI for nuclear staining. Images shown at 400 x original magnification are representative for results obtained with cells from 3 independent experiments. (e) Immunofluorescence staining at 72 hpi, with antibodies against acetylated α-tubulin (ciliated cell marker) or MUC5AC (goblet cell marker) in combination with anti-SARS-CoV-2 N protein antibody (JUC3) and DAPI for nuclear staining. Immunofluorescence images shown are representative for results of 3 independent experiments with 630 x original magnification. (f) Immunofluorescence staining with antibodies against MUC5AC and FOXJ1 (ciliated cell marker) with anti-SARS-CoV-2 N protein antibody and DAPI for nuclear staining. Immunofluorescence images shown are representative for results of 3 independent experiments with 400 x original magnification. (g) Quantification of immunostaining of $FOXJ1^+$, $MUC5AC^+$ and $FOXJ1^+MUC5AC^+$ or other cells in cultures of two single donors was performed with Image J software.

Modulating epithelial cellular composition has moderate effects on SARS-CoV-2 infection

To further explore the association between epithelial cellular composition and viral infection, we skewed cellular differentiation of ALI-PBEC during the last 2 weeks of differentiation to either an enrichment in ciliated cells at the cost of goblet cells, or towards an enrichment in goblet cells at the expense of ciliated cells using DAPT or interleukin 13 (IL-13), respectively (29, 44, 45). We infected these cultures with

SARS-CoV-2 to analyse if enrichment in one of these cell types impacted infection kinetics. We could verify that DAPT treatment caused a marked increase in the number of ciliated cells (FOXJ1^{+} and acetylated α-tubulin^{+}), while the number of goblet cells (MUC5AC^{+}) was decreased (Fig. 2a and S2a). Conversely, IL-13 treatment increased the fraction of goblet cells and decreased the number of ciliated cells (Fig. 2A and S2A), also confirmed at gene expression level (Fig. S2b). Additionally, a small percentage of FOXJ1 and MUC5AC double-positive transient secretory cells was detected in all cultures, which was not significantly affected by IL-13 or DAPT treatment (Figure S2a).

We infected these DAPT- or IL-13-treated cultures with SARS-CoV-2 and in line with the data shown in Fig. 1, detected by immunofluorescence staining that only a few cells were infected at 24 hpi in untreated and treated cultures (Fig. 2b). At 48 and 72 hpi, all cultures showed an increase in viral load compared to 24 hpi (Fig. 2b), demonstrating that viral infection and replication was feasible in all cultures despite the significant change in cellular composition between these conditions. In IL-13-treated cell cultures, intracellular viral RNA levels were highest at 48 hpi, while being similar to control again at 72 hpi (Fig. 2c). To our surprise the level of intracellular SARS-CoV-2 RNA was lower in DAPT-treated cells at all time points compared to the controls (Fig. 2c). Similar trends were found for the release of infectious particles, as shown in Fig. 2d. When we checked for cell types infected with SARS-CoV-2 in DAPT-treated cultures, due to the lack of goblet cells, ciliated cells were the only identified cells. In IL-13-treated cultures we observed infection of ciliated and goblet cells, similar to control cultures. (Fig. 2e).

To exclude the possibility that the effects observed in DAPT-treated cultures were a direct consequence of inhibition of Notch signalling rather than epithelial remodelling, we treated cells with DAPT either starting 24 h before (and during) infection (a time period considered insufficient to cause a shift in epithelial differentiation) or directly after infection. These short-term treatments with DAPT did not result in significant changes in the intracellular viral RNA copies or production of infectious progeny, suggesting that inhibition of Notch signalling itself has no direct effect on SARS-CoV-2 replication (Fig. S2c). These data suggest that rather than one cell-type alone, possibly the interplay between goblet and ciliated cells is important for susceptibility of ALI-PBEC to SARS-CoV-2 infection.

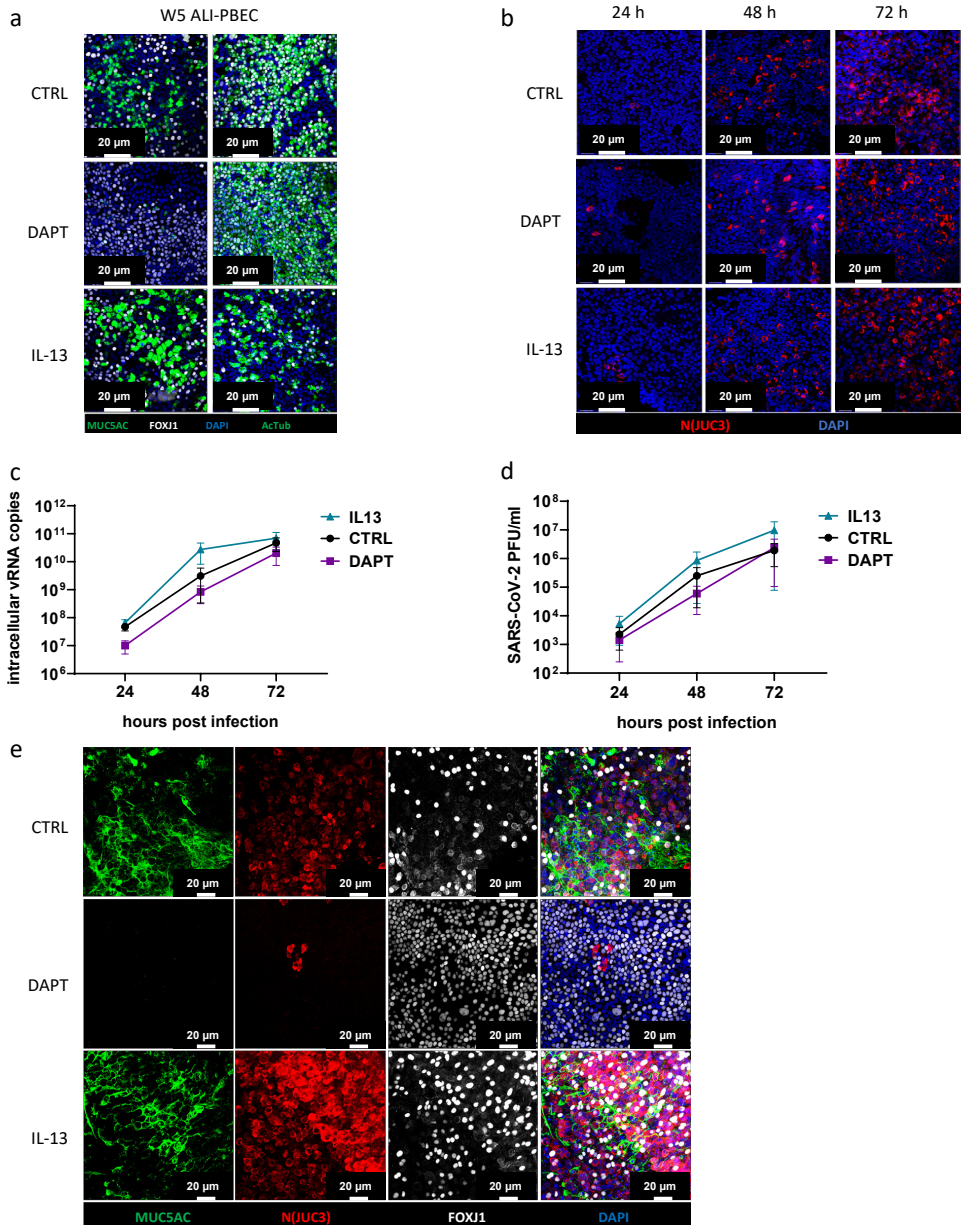

Figure 2. Effect of IL-13 treatment, and DAPT-mediated inhibition of Notch signaling on epithelial susceptibility to SARS-CoV-2 infection. ALI-PBEC (mix of 4-5 donors) were differentiated for 3 weeks, before addition of DAPT (5 µM) or IL-13 (1 ng/ml) and differentiation for an additional 2 weeks. (a) After in total 5 weeks of differentiation, ALI-PBEC were fixed, stained using primary antibodies against MUC5AC and FOXJ1 (goblet cell marker, ciliated cell marker) or acetylated α-tubulin together with FOXJ1 (ciliated cell markers) in combination with DAPI for nuclear staining and analyzed by

immunofluorescence microscopy and quantified by ImageJ. (b) SARS-CoV-2 infected cells were stained with primary antibodies against SARS-CoV-2 N protein (JUC3) in combination with DAPI for nuclear staining. (c) Intracellular viral RNA copies were measured by RT-qPCR. (d) Plaque assay was performed to titrate viral progeny in the apical washes. n=3 independent experiments derived from 3 different donor mixes. Data are mean ± SEM. Analysis of differences was conducted using two-way ANOVA with a Tukey/Bonferroni post-hoc test. Significant differences are indicated by *P<0.05 compared with untreated samples. (e) Immunostaining of control, DAPT- or IL-13-treated cultures at 72 hpi with antibodies against MUC5AC (goblet cell marker), FOXJ1 (ciliated cell marker) and SARS-CoV-2 N protein in combination with DAPI for nuclear staining. Immunofluorescence images shown are representative for results of 3 independent experiments with 400 x original magnification.

Origin and culture duration of human airway epithelial cells affect SARS-CoV-2 infection

Next, we wanted to investigate how differentiation time and anatomical origin of the epithelial cultures affected SARS-CoV-2 infection biology. To this end, we employed cells isolated from bronchial or tracheal tissue and allowed ALI-PBEC and ALI-PTEC to differentiate for 3, 4 or 5 weeks, after which they were infected with 30,000 PFU of SARS-CoV-2. Viral load was analysed at 72 hpi. In both ALI-PBEC and ALI-PTEC, an increase in intra- and extracellular viral RNA as well as infectious virus particles was observed with longer differentiation time, with the highest viral load observed in cultures differentiated for 5 weeks after start of ALI (Fig. 3a-3c). A gradual 1-2 log increase in SARS-CoV-2 progeny production was observed when cultures had been differentiated up to 5 weeks when compared to 3 weeks of differentiation (Fig. S3a). Immunofluorescence staining of these cultures for the viral nucleocapsid protein also demonstrated an increase in the number of infected cells with increasing culture duration (Fig. 3c). Significantly higher viral load was observed in ALI-PBEC compared to ALI-PTEC, with an average 10-fold difference in extracellular SARS-CoV-2 RNA copies (Fig. 3a-3b) and infectious progeny (Fig. 3c), in particular in 5-week differentiated cultures. In conclusion, our results show that both the anatomical origin of the epithelial cells and the culture duration had a profound effect on the susceptibility of airway epithelial cells to SARS-CoV-2 infection.

Time of culturing affects the proportion of cell types related to mucociliary clearance

Since we found increased viral infection upon prolonged differentiation time and additionally we observed that SARS-CoV-2 infection targets mostly ciliated cells, goblet cells and transient secretory cells (which we also confirmed for ALI-PTEC (Fig. S3c)), we hypothesized that these target cells changed over time of differentiation. We compared cellular composition between 3, 4 and 5 week-differentiated cultures and found that these cultures at all time points expressed markers related to all dominant epithelial cell types (ciliated, goblet, club and basal cells) in ALI-PBEC and

PTEC (Fig. S3b). However, there were clear differences in the proportions of goblet and ciliated cells over time of differentiation (Fig. 3d). Using FOXJ1 and acetylated α-tubulin as markers for ciliated cells, we observed that the percentage of FOXJ1$^+$ cells was significantly higher in ALI-PBEC after 5-week culture compared to 3-week cultures. Also the percentage of ciliated cells was significantly higher in ALI-PBEC than in ALI-PTEC at all culture durations (Fig. 3e). The change in the percentage of MUC5AC$^+$ goblet cells was not significant over time in ALI-PBEC and ALI-PTEC (Fig. 3e). Additionally, the number of transient secretory cells was higher in ALI-PBEC than in ALI-PTEC (Fig. 3e). Furthermore, mRNA levels of *FOXJ1* were significantly increased in 4 week ALI-PBEC compared to 3 week cultures, however they did not further increase in 5 week cultures (Fig. S3d). In addition, *FOXJ1* mRNA was higher in 4/5-week ALI-PBEC cultures compared to 4/5-week PTEC cultures (Fig. S3d). *MUC5AC* mRNA levels were higher at week 5 in ALI-PTEC cultures compared to week 3, and also higher than in week 5 ALI-PBEC (Fig. S3d). In contrast, there was no significant difference in the expression of *SCGB1A1* (club cell marker) and *TP63* (basal cell marker) (Fig. S3d). These results suggest that despite the early presence of transcripts which are specific for certain cell types, differentiation of certain cell types (which also requires expression at the protein level) continues for several weeks in cultures at ALI. Altogether, we found differences in the percentage of ciliated cells between PTEC and PBEC and between cultures that differed in their incubation time at ALI, which was in line with differences in viral load.

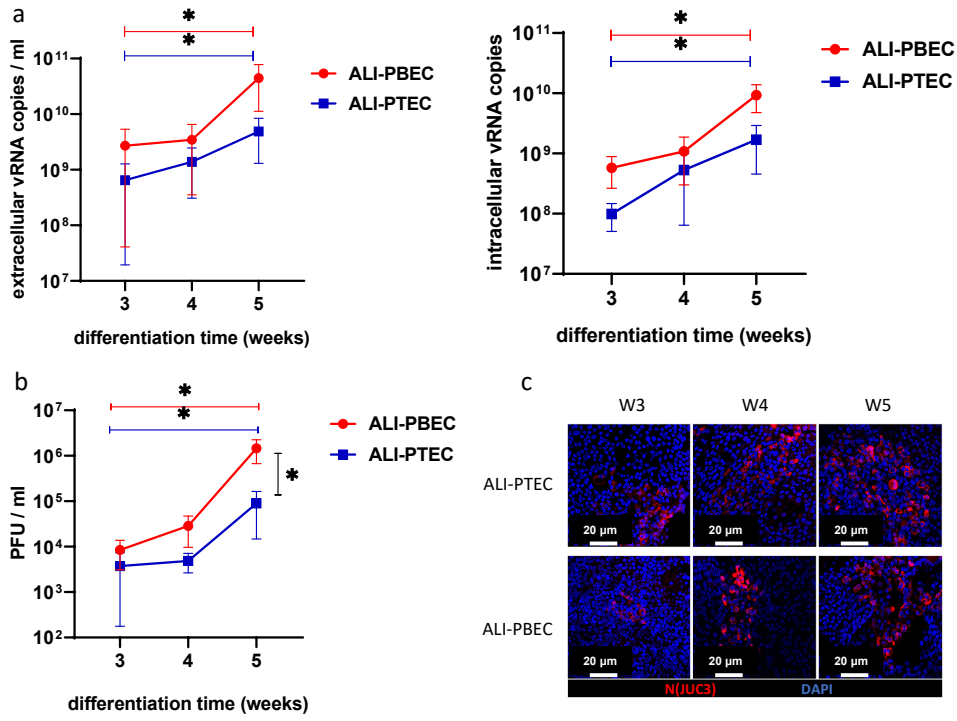

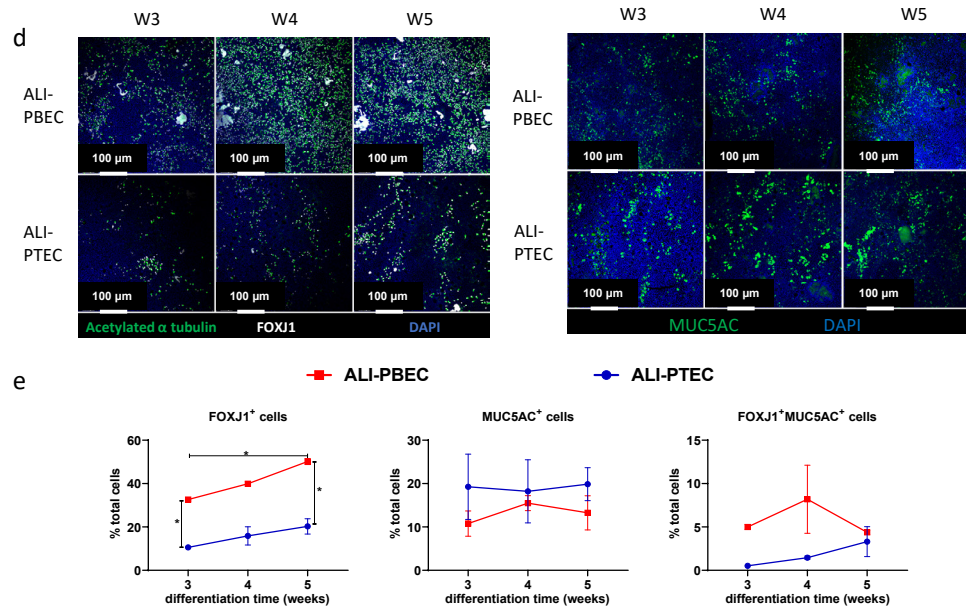

Figure 3. Effect of culture duration on SARS-CoV-2 infection in PTEC and PBEC. ALI-PBEC/ALI-PTEC (mix of 5 donors) cultured for 3-5 weeks were infected with SARS-CoV-2 (30,000 PFU per insert). (a) Extracellular viral RNA copies in the apical wash or intracellular copies were measured by RT-qPCR. (b) Viral infectious progeny was determined by plaque assay in Vero E6 cells. Mean values ± SEM is presented from 3 independent experiments using 3 different donor mixes. Statistical analysis was conducted using two-way ANOVA with a Tukey/Bonferroni post-hoc test. Significant differences are indicated by *P<0.05. (c) Cells were immunofluorescence stained with rabbit polyclonal anti-SARS-CoV-2 N protein antibody (JUC3) and DAPI for nuclear staining. Images shown are representative for results obtained with ALI-PBEC and ALI-PTEC from the same 3 independent experiments shown in A-B at 400 x original magnification. (d) Immunofluorescence staining of 3, 4, 5 week cultures using antibodies against acetylated α-tubulin and FOXJ1 (ciliated cell markers) or MUC5AC (goblet cell marker) in combination with DAPI for nuclear staining. Images shown are representative for results of 3 independent experiments with 100x/400x (insert) original magnification. (e) Quantification of FOXJ$^+$, MUC5AC$^+$ cells and FOXJ1$^+$MUC5AC$^+$ cells was done by Image J software.

Changes in gene expression associated with SARS-CoV-2 target cells

To further explore the gradual increase in susceptibility to SARS-CoV-2 infection with longer culture time, we compared the expression profiles of 3-week and 5-week uninfected differentiated cultures by bulk RNA-Seq and applied cellular deconvolution. We identified 169 differentially expressed genes, of which expression of 49 genes were upregulated while expression of 120 genes was downregulated in ALI-PBEC at 5 vs 3 weeks (Fig. 4a and Table S1). In ALI-PTEC, the expression of 32 genes increased, and 26 genes showed decreased expression in 5-week cultures compared to 3-week cultures (Fig. 4b and Table S1). Gene set enrichment analysis

was conducted to identify the top differentially upregulated and downregulated gene sets in ALI-PBEC between week 5 and week 3 (Table 2). A striking difference in ALI-PBEC between week 5 and week 3 was observed for the gene sets related to markers of ciliated and basal cells. Cellular deconvolution analysis further showed that the relative proportion of ciliated cells was increased in 5-week ALI-PBEC cultures and the same trend was also found for ALI-PTEC (Fig. 4c and 4d). Altogether, RNA-Seq analysis did not reveal additional changes in cell types between the 3 and 5 week culture duration.

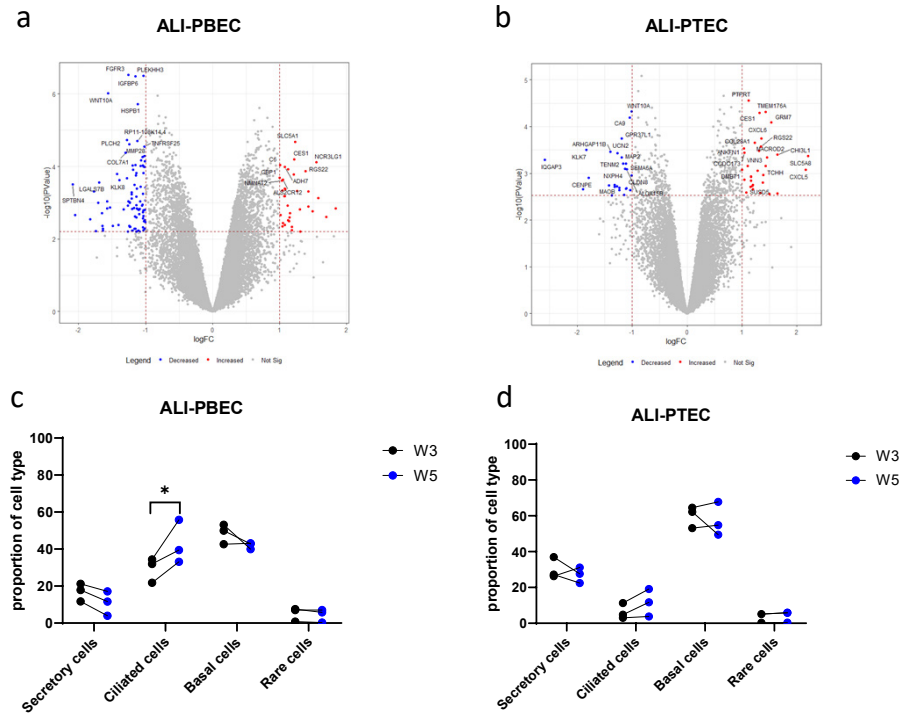

Figure 4. Transcriptional responses comparing 3 and 5 weeks-differentiated primary bronchial and tracheal cells using RNA-Seq analysis. PBEC and PTEC were cultured at ALI for 3 weeks or 5 weeks. Then RNA was isolated from these samples and used for RNA-Seq analysis. (a-b) Volcano plots depicting changes in the gene expression profiles of 5-week cultures compared to 3-week cultures from ALI-PBEC or ALI-PTEC. The DEGs were considered significant when they had a Benjamini Hochberg p value<0.1 and a fold change>|2. Genes depicted in red are significantly upregulated while genes depicted in blue are significantly downregulated in 5-week cultures compared to 3-week cultures in ALI-PBEC (a) or ALI-PTEC (b). (c-d) The relative proportion of different cell types for each donor mix in ALI-PBEC (c) cultures and ALI-PTEC (d) cultures as determined by cellular deconvolution of the transcriptomic datasets.

Direction	Gene Set Name	# Genes in Gene Set (K)	Description	# Genes in Overlap (k)	k/K	p-value	FDR q-value
Upregulated	MURARO_PANCREAS_DUCTAL_CELL	1276		12	0.0094	9.25E-9	1.79E-4
Upregulated	GOBP_DEFENSE_RESPONSE	1739	Reactions, triggered in response to the presence of a foreign body or the occurrence of an injury, which result in restriction of damage to the organism attacked or prevention/recovery from the infection caused by the attack. [GOC:go_curators]	12	0.0069	2.7E-7	2.3E-3
Upregulated	WP_PROXIMAL_TUBULE_TRANSPORT	58	Proximal tubule transport	4	0.0690	5.25E-7	2.3E-3
Upregulated	WP_NRF2_PATHWAY	145	NRF2 pathway	5	0.0345	5.77E-7	2.3E-3
Upregulated	DESCARTES_FETAL_INTESTINE_INTESTINAL_EPITHELIAL_CELLS	276	descartes DE_gene_by_organ.csv, fold.change>5, qval<0.05, pval<0.05	6	0.0217	5.94E-7	2.3E-3
Upregulated	REACTOME_G_ALPHA_I_SIGNALLING_EVENTS	314	G alpha (i) signalling events	6	0.0191	1.26E-6	3.46E-3
Upregulated	GOMF_SOLUTE_SODIUM_SYMPORTER_ACTIVITY	72	Enables the transfer of a solute or solutes from one side of a membrane to the other according to the reaction: solute(out) + Na+(out) = solute(in) + Na+(in). [GOC:ai]	4	0.0556	1.26E-6	3.46E-3
Upregulated	WP_NUCLEAR_RECEPTORS_METAPATHWAY	321	Nuclear receptors meta-pathway	6	0.0187	1.43E-6	3.46E-3
Upregulated	**TRAVAGLINI_LUNG_CILIATED_CELL**	**1094**		**9**	**0.0082**	**2.59E-6**	**5.57E-3**
Upregulated	TRAVAGLINI_LUNG_MACROPHAGE_CELL	201		5	0.0249	2.88E-6	5.58E-3
Downregulated	GOCC_SUPRAMOLECULAR_COMPLEX	1329	A cellular component that consists of an indeterminate number of proteins or macromolecular complexes, organized into a regular, higher-order structure such as a polymer, sheet, network or a fiber. [GOC:dos]	18	0.0135	9.81E-9	8.53E-5
Downregulated	**TRAVAGLINI_LUNG_PROLIFERATING_BASAL_CELL**	**891**		**15**	**0.0168**	**1.12E-8**	**8.53E-5**
Downregulated	HAY_BONE_MARROW_STROMAL	767		14	0.0183	1.32E-8	8.53E-5

Downregulated	**TRAVAGLINI_ LUNG_BASAL_CELL**	**188**		**8**	**0.0426**	**3.6E-8**	**1.61E-4**
Downregulated	GOCC_SUPRAMOLECULAR_POLYMER	996	A polymeric supramolecular structure. [GOC:dos]	15	0.0151	4.84E-8	1.61E-4
Downregulated	ZHONG_PFC_C2_ UNKNOWN_NPC	76		6	0.0789	5.04E-8	1.61E-4
Downregulated	HALLMARK_KRAS_ SIGNALING_DN	200	Genes down-regulated by KRAS activation.	8	0.0400	5.81E-8	1.61E-4
Downregulated	NABA_ MATRISOME	1026	Ensemble of genes encoding extracellular matrix and extracellular matrix-associated proteins	15	0.0146	7.1E-8	1.72E-4
Downregulated	MANNO_MIDBRAIN_NEUROTYPES_ HNPROG	229	Cell types are named using anatomical and functional mnemonics prefixed by 'm' or'h' to indicate mouse and human respectively: OMTN, oculomotor and trochlear nucleus; Sert, serotonergic; NbM, medial neuroblast; NbDA, neuroblast dopaminergic; DA0-2, dopaminergic neurons; RN, red nucleus; Gaba1-2, GABAergic neurons; mNbL1-2, lateral neuroblasts; NbML1-5, mediolateral neuroblasts; NProg, neuronal progenitor; Prog, progenitor medial floorplate (FPM), lateral floorplate (FPL), midline (M), basal plate (BP); Rgl1-3, radial glia-like cells; Mgl, microglia; Endo, endothelial cells; Peric, pericytes; Epend, ependymal; OPC, oligodendrocyte precursor cells.	8	0.0349	1.64E-7	3.45E-4
Downregulated	FAN_EMBRYONIC_ CTX_MICROGLIA_1	155		7	0.0452	1.78E-7	3.45E-4

Table 2: Top 10 gene sets of the differentially expressed genes analyzed using gene set enrichment analysis (GSEA). P value was calculated from the hypergeometric distribution for (k-1, K, N - K, n) where k is the number of genes in the intersection of the query set with a set from MSigDB; K is the number of genes in the set from MSigDB; N is the total number of gene universe (all known human gene symbols); n is the number of genes in the query set. FDR q-value means the false discovery rate analog of hypergeometric p-value after correction for multiple hypothesis testing according to Benjamini and Hochberg. The gene sets related to cellular composition of lung are highlighted in bold.

Cell culture duration alters expression of SARS-CoV-2 entry factors

The expression of host proteins that have been linked to entry of SARS-CoV-2 varies between the different airway epithelial cell types (23). Therefore, we investigated whether the observed increase in susceptibility to SARS-CoV-2 with increased differentiation time and the effect of the anatomical origin, was related to the expression of the main receptor ACE2, or other factors involved in entry. We compared the mRNA levels of different viral entry factors between the single-donor cultures that displayed the highest and lowest viral load (Fig. 1a, Fig. 5a). Interestingly,

the culture with the highest viral load expressed higher mRNA levels of *CTSL* and *TMPRSS2* at baseline, while other factors did not differ. Furthermore, we assessed the expression of cell-entry factors in cultures of varying differentiation time using our RNA-Seq dataset (Fig. 5b). In both ALI-PBEC and ALI-PTEC cultures, there was a significant increase in expression of *TMPRSS2* in 5-week cultures compared to 3-week cultures. In addition, expression of *CTSL* was significantly increased while expression of *CD147* was decreased at 5 weeks compared to 3 weeks in ALI-PBEC. However, expression of *NRP1* was reduced at 5 weeks compared to 3 weeks in ALI-PTEC, and expression of *ACE2*, *FURIN* and *NRP1* was lower in 3-week ALI-PBEC compared to 3-week ALI-PTEC (Fig. 5b). We compared the expression of these genes by RT-qPCR in 3- and 5-week cultures, and also included 4-week cultures (Fig. S4a). With longer culture duration, in both ALI-PBEC and ALI-PTEC, gene expression of *CTSL* and *TMPRSS2* indeed increased over time and a significant increase was found in expression of *TMPRSS2* in 4-week ALI-PBEC compared to 3-week cultures. Gene expression of *ACE2* and *GRP78* did not change with culture duration. A significant increase in expression of *CD147* was observed in 4-week ALI-PBEC compared to 3-week cultures (Fig. S4a). Treatment with DAPT or IL-13 did not affect expression of SARS-CoV-2 entry factors (Fig. S4b). These findings indicated that changes in expression of *CTSL* and *TMPRSS2* could (in part) be responsible for the observed differences in susceptibility to SARS-CoV-2 infection between 3-, 4- and 5-week differentiated cultures.

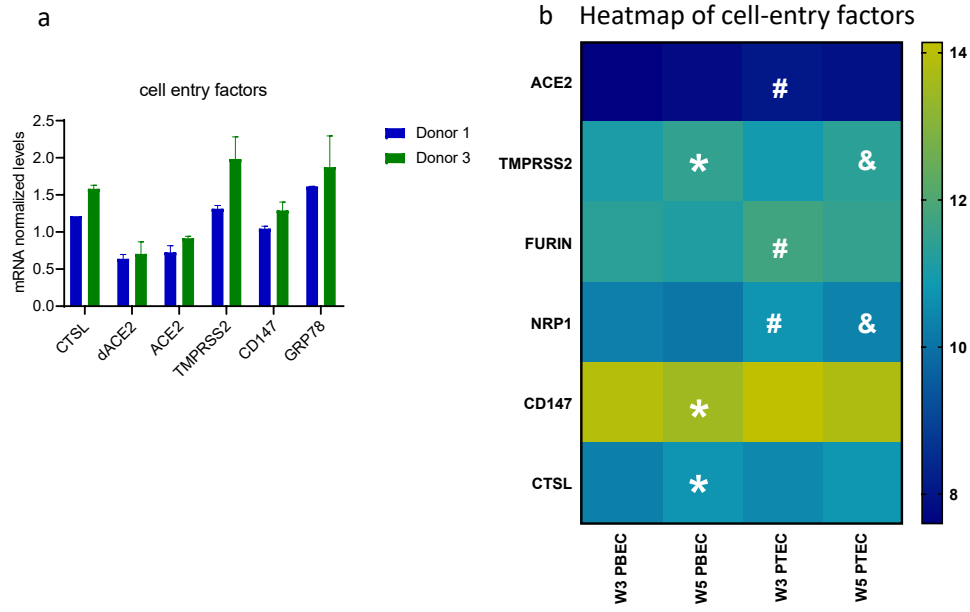

Figure 5. Effect of donor variation and culture duration on expression of SARS-CoV-2 cell-entry factors. (a) RT-qPCR analysis of gene expression of viral cell-entry factors in two single donor cultures at 5 weeks. Data are mean values ± SEM. n=2 duplicated wells per donor. (b) Heatmap of transcriptional

changes (RNA-Seq data) of SARS-CoV-2 cell-entry factors in 3-week and 5-week PBEC and PTEC. Differences were assessed by a two-way ANOVA with Tukey's test and the significant difference were considered at $P < 0.05$. *= 5-week ALI-PBEC vs 3-week ALI-PBEC; &=5-week ALI-PTEC vs 3-week ALI-PTEC; #=3-week ALI-PTEC vs 3-week ALI-PBEC.

Cell culture duration does not affect SARS-CoV-2-induced antiviral responses

Antiviral responses in the epithelium are critical for protection against viral infections. Therefore, we investigated whether antiviral responses changed depending on the ALI culture duration, and whether this could provide an additional explanation of the observed increased susceptibility to infection with longer culture times. In ALI-PTEC, SARS-CoV-2-induced mRNA levels of both *IFNB1* and *IFNL1* increased significantly with culture duration. When cultures were infected at week 3 or 4 there was little *IFNB1* or *IFNL1* mRNA produced, while expression of these genes was strongly upregulated by SARS-CoV-2 infection in 5 week old cultures (Fig. S5a and S5b). Gene expression analysis of *IFNB1* and *IFNL1* showed a similar increasing trend in ALI-PBEC upon infection (Fig. S5c and S5d). When 5-week PBEC were (long-term) treated with DAPT, we observed lower SARS-CoV-2-induced antiviral responses than in untreated and IL-13-treated cultures (Fig. S5e and 5f). All these findings correlate with the observed differences in the number of infected cells and viral load resulting from culture duration and DAPT and IL-13 treatment (Fig. 2). This suggests that antiviral responses were not affected by differentiation time or long-term DAPT/IL-13 treatment, but rather differed as a direct consequence of differences in the level of infection.

Discussion

The Discussion/Conclusion should provide an evaluation of the results. There should be a clear Here we investigated the influence of cellular composition and differentiation of human primary airway epithelial cell cultures on SARS-CoV-2 infection biology. Our key finding is that changes in cell types related to mucociliary clearance, i.e. ciliated and goblet cells, influence SARS-CoV-2 infection of human primary airway epithelial cells. Specifically, a higher percentage of ciliated cells appears to be the main contributing factor to a higher level of infection. This is likely a consequence of their higher susceptibility to infection in comparison to the other cell-types, and possibly their contribution to spreading of virus across the epithelial surface of the culture. Nevertheless, our data also suggest that the presence of mucus and/or goblet cells is important, since a reduction in goblet cells reduced viral load, even in cultures with a higher percentage of ciliated cells. Finally, we provide experimental evidence for infection of transient secretory cells by SARS-CoV-2.

With regard to differentiation time, there is no golden standard protocol for ALI-

primary airway epithelial cell cultures to obtain cultures that best resemble the human epithelial cellular composition. Literature reports that differentiation times anywhere between 2 and 6 weeks after start of air-liquid interface culture are needed to have all key cell-types present in culture (19, 20, 46).

In line with a recent study investigating SARS-CoV-2 infection using primary airway epithelial cells(19), and based on our own study comparing 3-5 week old cultures, we decided to use 5 weeks differentiated ALI-PBEC cultures. We found a reproducible increase in viral titers over time post infection. In addition, cultures of well-differentiated airway epithelial cells adequately model *in vivo* host antiviral responses (47, 48), which we could confirm also for SARS-CoV-2 infection by detecting increased mRNA levels of *IL-6* and *CXCL8*. In contrast, downregulated expression of *IL-6* and *CXCL8* was reported in the human bronchial epithelial cell line 16HBE (49).

We confirmed that both ciliated and goblet cells were infected by SARS-CoV-2 in our ALI- cultures, whereas almost no infected club and basal cells were detected (data not shown). This is consistent with results from recent studies looking into the cellular tropism of SARS-CoV-2 showing infection of multiple epithelial cell types, among them ciliated cells, goblet cells and club cells of the airway epithelium, and type 2 alveolar epithelial cells (19, 20, 50, 51). Additionally, we also observed cells co-expressing markers of ciliated cells (FOXJ1) and goblet cells (MUC5AC) in our cultures. This specific cell population, which was recently reported by e.g. Garcia *et al.* (52) and by Vieira Braga et al (53), is suggested to represent a transitional state between goblet and ciliated cells, and was recently labelled as transient secretory cells (26). Based on their relatively high co-expression of ACE2 and TMPRSS2, Lukassen et al. (26) suggested that these transient secretory cells may be particularly vulnerable to SARS-CoV-2 infection. Whereas we showed for the first time that SARS-CoV-2 was also able to infect these cells, it remains unknown if the low percentage of these cells in our culture model significantly contributed to the overall level of infection. Considering the role in mucociliary clearance of ciliated, goblet and potentially transient secretory cells, we conclude that cells involved in mucociliary clearance are predominantly infected by SARS-CoV-2.

To investigate the role of cellular composition in susceptibility to viral infection, we skewed cell differentiation with the Notch signalling inhibitor DAPT (44), which resulted in cultures that constituted a high number of ciliated cells but lacked goblet cells and transient secretory cells. Surprisingly the viral load in these cultures was reduced compared to untreated cultures. A possible explanation would be that ciliated cells become infected by the virus, and mucus produced by goblet cells helps spread the infection after release and therefore hinders clearance by ciliated cells, which would be consistent with previous findings that SARS-CoV-2 infects ciliated cells with attached mucus (54). Conversely, the modulation with IL-13, (slightly)

increased viral loads compared to control and DAPT-treated cultures, which is in line with the suggestion from other studies that patients with allergic asthma, a disease associated with IL-13-induced changes in epithelial cell composition, may be somewhat more susceptible to SARS-CoV-2 infection (55). Others have observed that treatment with IL-13 reduced viral RNA copies in ALI-cultured airway epithelial cells (56, 57). There is no clear explanation for this discrepancy, although the reduced levels of *ACE2* after IL-13 treatment that were found in these studies might have been responsible for the reduced infection levels. However, in our studies ACE2 was not affected by IL-13 treatment. Furthermore, we used a much lower MOI (0.03 versus 0.5), therefore even if a reduction in the main target cells (e.g. ciliated cells) was achieved by IL-13, a lower MOI would not likely be rate-limiting for this low infection level. Collectively, these observations indicate that DAPT- and IL-13-mediated modulation of epithelial cell differentiation does not provide a simple link between differences in epithelial cell composition and susceptibility to SARS-CoV-2 infection. A combination of factors appears to play a role, for example mucus secretion by goblet cells (58), which – if excessive - could hinder clearance of the virus in the epithelium. We therefore used additional approaches to study the contributing effect of cellular composition to SARS-CoV-2 infection. We could demonstrate that changes in cellular composition either linked to anatomical origin, donor or culture time, influenced SARS-CoV-2 infection. The shared outcome was that for each variable the amount of target cells correlated to the viral load, suggesting that the percentage of ciliated cells is a strong contributing factor to the SARS-CoV-2 infection rate.

Considering that expression of viral entry factors varies between different cell types, we furthermore investigated their expression in cells from different donors, the effect of culture duration, and the impact of treatment with DAPT and IL-13. According to literature, all main cell types express *TMPRSS2,* whereas transient secretory cells most strongly co-expressed *TMPRSS2* (26). *CTSL* gene expression was reported to be higher in ciliated cells compared to other epithelial cell types (59). When we compared two single donors, cell cultures isolated from one donor expressed more *CTSL* and *TMPRSS2,* which was in line with the observed higher viral replication and higher abundance of ciliated cells in this donor. Furthermore, an increased expression of *CTSL* as well as *TMPRSS2* was also found with prolonged culture duration. Thus, the difference in *CTSL* expression could link to changes in the ciliated cell number, which supports the role of ciliated cells in viral replication. Furthermore in line with this, CTSL levels were recently found to be positively correlated with severity of disease in COVID-19 patients, pointing to its role in enhancement of infection (60). We excluded possible effects of changes in antiviral responses on the gradual increase in viral infection with the prolonged culture duration since, we did not observe lower expression of type I and III IFNs over culture time at ALI, but rather found a correlation with the level of viral replication.

Our study demonstrates that the use of mixed donor cultures is an efficient way to recapitulate natural variability between donors while saving on resources (cells, culture plastics and media) that are in high demand/short supply. The level of donor-to-donor variation was also represented in inter-experimental variation when using the same donor mix. It needs to be noted that the comparison between PBEC and PTEC in this study needs to be interpreted with caution, because PBEC were derived from tumor-free resected bronchial tissue from (ex-) smoking patients with lung cancer, and PTEC were from donor lungs without lung disease.

Overall, in this study we have established that epithelial cell types related to mucociliary clearance (i.e. ciliated, goblet cells and transient secretory cells) seem pivotal for SARS-CoV-2 infection and spread of the infection over the epithelial tissue. This study underlines the importance of assessing these cell types and the role of mucus when studying how SARS-CoV-2 infection biology is affected in patients with chronic lung disease, such as those with chronic type 2 inflammation in asthma or in COPD, where epithelial remodelling likely has shifted these cell-type ratios.

Statements

A preprint version of this article is available on bioRxiv (61).

Statement of Ethics

Patients from which this PBEC were derived were enrolled in the biobank via a no-objection system for coded anonymous further use of such tissue (www.coreon.org). However, since 29-11-2020, patients have been enrolled in the biobank using active informed consent in accordance with local regulations from the LUMC biobank with approval by the institutional medical ethical committee (B20.042/Ab/ab and B20.042/Kb/kb). For the present study, cells from patients were used that were collected before 29-11-2020, and based on the regulations of the no-objection system, individual informed consent was not needed. PTEC were isolated from residual tracheal and main stem bronchial tissue from lung transplant donors post-mortem at the University Medical Center Essen (Essen, Germany). Use of such donor tissue for research was approved by the ethical committee of the Medical faculty of the University Duisburg-Essen (ID: 19-8717-BO). Informed consent for the use of PTEC was provided by the transplant recipients of the respective lungs.

Conflict of Interest Statement

The authors have no conflicts of interest to declare.

Funding Sources

This study was supported by a COVID-19 MKMD grant from the Netherlands Organization for Health Research and Development (ZonMw) and the Dutch Society for the Replacement of Animal Testing (Stichting Proefdiervrij) (grant #114025007). C.S.-B. was supported by the Coordination for the Improvement of Higher Education Personnel (CAPES) (process no. 88881.171440/2018-01), Ministry of Education, Brazil. Part of this research was supported by the Leiden University Fund (LUF), the Bontius Foundation, and donations from the crowdfunding initiative “wake up to corona”. This study has also received funding from the European Union’s Horizon 2020 research and Innovation program under grant No 10100362 (the SCORE project). Part of RNA-Seq and analysis was supported by a RSEOH-CAG Rapid Response Research Initiative and a RSEOH-CAG 2021 Extension Grant. Collection of primary human tracheal epithelial cells was supported by grants from the Deutsche Forschungsgemeinschaft (DFG) (Ta 275/7-1 and Ta 275/8-1) to C.T.

Author Contributions

Melissa Thaler, Ying Wang, Anne M. van der Does, Pieter S. Hiemstra and Martijn J. van Hemert were involved in study design and conceptualization. Melissa Thaler, Ying Wang, Dennis K. Ninaber, Natacha S. Ogando, Clarisse Salgado-Benvindo performed experiments. Alen Faiz performed RNA-Seq analysis and cellular deconvolution. Hendrik Beckert, Christian Taube collected and isolated human tracheal epithelial cells. Melissa Thaler and Ying Wang wrote the manuscript. Anne M. van der Does, Pieter S. Hiemstra and Martijn J. van Hemert revised the manuscript. The final version was critically reviewed and approved by all authors.

Data Availability Statement

Data are available upon reasonable request by sending a message to the corresponding author.

References

1. Chakraborty I, Maity P. COVID-19 outbreak: Migration, effects on society, global environment and prevention. Sci Total Environ. 2020;728:138882.
2. Yurkovetskiy L, Wang X, Pascal KE, Tomkins-Tinch C, Nyalile TP, Wang Y, et al. Structural and Functional Analysis of the D614G SARS-CoV-2 Spike Protein Variant. Cell. 2020;183(3):739-51.e8.
3. Toyoshima Y, Nemoto K, Matsumoto S, Nakamura Y, Kiyotani K. SARS-CoV-2 genomic variations associated with mortality rate of COVID-19. J Hum Genet. 2020;65(12):1075-82.
4. Trevisan C, Noale M, Prinelli F, Maggi S, Sojic A, Di Bari M, et al. Age-Related Changes in Clinical Presentation of Covid-19: the EPICOVID19 Web-Based Survey. Eur J Intern Med. 2021;86:41-7.
5. Alwani M, Yassin A, Al-Zoubi RM, Aboumarzouk OM, Nettleship J, Kelly D, et al. Sex-based differences in severity and mortality in COVID-19. Rev Med Virol. 2021;31(6):e2223.
6. Yu W, Rohli KE, Yang S, Jia P. Impact of obesity on COVID-19 patients. J Diabetes Complications. 2021;35(3):107817.
7. Carraturo F, Del Giudice C, Morelli M, Cerullo V, Libralato G, Galdiero E, et al. Persistence of SARS-CoV-2 in the environment and COVID-19 transmission risk from environmental matrices and surfaces. Environ Pollut. 2020;265(Pt B):115010.
8. Bansal M. Cardiovascular disease and COVID-19. Diabetes Metab Syndr. 2020;14(3):247-50.
9. Ovsyannikova IG, Haralambieva IH, Crooke SN, Poland GA, Kennedy RB. The role of host genetics in the immune response to SARS-CoV-2 and COVID-19 susceptibility and severity. Immunol Rev. 2020;296(1):205-19.
10. Park SE. Epidemiology, virology, and clinical features of severe acute respiratory syndrome -coronavirus-2 (SARS-CoV-2; Coronavirus Disease-19). Clin Exp Pediatr. 2020;63(4):119-24.
11. Zhou P, Yang X-L, Wang X-G, Hu B, Zhang L, Zhang W, et al. A pneumonia outbreak associated with a new coronavirus of probable bat origin. Nature. 2020;579(7798):270-3.
12. Iwasaki A, Foxman EF, Molony RD. Early local immune defences in the respiratory tract. Nat Rev Immunol. 2017;17(1):7-20.
13. Hiemstra PS, McCray PB, Jr., Bals R. The innate immune function of airway epithelial cells in inflammatory lung disease. Eur Respir J. 2015;45(4):1150-62.
14. Iwasaki A, Foxman EF, Molony RD. Early local immune defences in the respiratory tract. Nature Reviews Immunology. 2017;17(1):7-20.
15. Bovard D, Giralt A, Trivedi K, Neau L, Kanellos P, Iskandar A, et al. Comparison of the basic morphology and function of 3D lung epithelial cultures derived from several donors. Curr Res Toxicol. 2020;1:56-69.
16. Belgacemi R, Luczka E, Ancel J, Diabasana Z, Perotin JM, Germain A, et al. Airway epithelial cell differentiation relies on deficient Hedgehog signalling in COPD. EBioMedicine. 2020;51:102572.
17. Leung C, Wadsworth SJ, Yang SJ, Dorscheid DR. Structural and functional variations in human bronchial epithelial cells cultured in air-liquid interface using different growth media. Am J Physiol Lung Cell Mol Physiol. 2020;318(5):L1063-l73.
18. Hou YJ, Okuda K, Edwards CE, Martinez DR, Asakura T, Dinnon KH, 3rd, et al. SARS-CoV-2 Reverse Genetics Reveals a Variable Infection Gradient in the Respiratory Tract. Cell. 2020;182(2):429-46.e14.
19. Zhu N, Wang W, Liu Z, Liang C, Wang W, Ye F, et al. Morphogenesis and cytopathic effect of

SARS-CoV-2 infection in human airway epithelial cells. Nat Commun. 2020;11(1):3910.
20. Hao S, Ning K, Kuz CA, Vorhies K, Yan Z, Qiu J. Long-Term Modeling of SARS-CoV-2 Infection of In Vitro Cultured Polarized Human Airway Epithelium. mBio. 2020;11(6).
21. Ehre C. SARS-CoV-2 Infection of Airway Cells. N Engl J Med. 2020;383(10):969.
22. Hoffmann M, Kleine-Weber H, Schroeder S, Krüger N, Herrler T, Erichsen S, et al. SARS-CoV-2 Cell Entry Depends on ACE2 and TMPRSS2 and Is Blocked by a Clinically Proven Protease Inhibitor. Cell. 2020;181(2):271-80.e8.
23. Sungnak W, Huang N, Bécavin C, Berg M, Queen R, Litvinukova M, et al. SARS-CoV-2 entry factors are highly expressed in nasal epithelial cells together with innate immune genes. Nat Med. 2020;26(5):681-7.
24. Aguiar JA, Tremblay BJ, Mansfield MJ, Woody O, Lobb B, Banerjee A, et al. Gene expression and in situ protein profiling of candidate SARS-CoV-2 receptors in human airway epithelial cells and lung tissue. Eur Respir J. 2020;56(3).
25. Wang S, Qiu Z, Hou Y, Deng X, Xu W, Zheng T, et al. AXL is a candidate receptor for SARS-CoV-2 that promotes infection of pulmonary and bronchial epithelial cells. Cell Research. 2021.
26. Lukassen S, Chua RL, Trefzer T, Kahn NC, Schneider MA, Muley T, et al. SARS-CoV-2 receptor ACE2 and TMPRSS2 are primarily expressed in bronchial transient secretory cells. Embo j. 2020;39(10):e105114.
27. Bridges JP, Vladar EK, Huang H, Mason RJ. Respiratory epithelial cell responses to SARS-CoV-2 in COVID-19. 2022;77(2):203-9.
28. Schrumpf JA, Ninaber DK, van der Does AM, Hiemstra PS. TGF-β1 Impairs Vitamin D-Induced and Constitutive Airway Epithelial Host Defense Mechanisms. Journal of innate immunity. 2020;12(1):74-89.
29. Wang Y, Ninaber DK, van Schadewijk A, Hiemstra PS. Tiotropium and Fluticasone Inhibit Rhinovirus-Induced Mucin Production via Multiple Mechanisms in Differentiated Airway Epithelial Cells. Front Cell Infect Microbiol. 2020;10:278.
30. Kovacikova K, Morren BM, Tas A, Albulescu IC, van Rijswijk R, Jarhad DB, et al. 6'-β-Fluoro-Homoaristeromycin and 6'-Fluoro-Homoneplanocin A Are Potent Inhibitors of Chikungunya Virus Replication through Their Direct Effect on Viral Nonstructural Protein 1. Antimicrob Agents Chemother. 2020;64(4).
31. Corman VM, Landt O, Kaiser M, Molenkamp R, Meijer A, Chu DK, et al. Detection of 2019 novel coronavirus (2019-nCoV) by real-time RT-PCR. Euro Surveill. 2020;25(3).
32. de Wilde AH, Raj VS, Oudshoorn D, Bestebroer TM, van Nieuwkoop S, Limpens R, et al. MERS-coronavirus replication induces severe in vitro cytopathology and is strongly inhibited by cyclosporin A or interferon-α treatment. The Journal of general virology. 2013;94(Pt 8):1749-60.
33. Graham C, Seow J, Huettner I, Khan H, Kouphou N, Acors S, et al. Neutralization potency of monoclonal antibodies recognizing dominant and subdominant epitopes on SARS-CoV-2 Spike is impacted by the B.1.1.7 variant. Immunity. 2021;54(6):1276-89.e6.
34. Mootha VK, Lindgren CM, Eriksson K-F, Subramanian A, Sihag S, Lehar J, et al. PGC-1α-responsive genes involved in oxidative phosphorylation are coordinately downregulated in human diabetes. Nature Genetics. 2003;34(3):267-73.
35. Subramanian A, Tamayo P, Mootha VK, Mukherjee S, Ebert BL, Gillette MA, et al. Gene set enrichment analysis: A knowledge-based approach for interpreting genome-wide expression profiles. Proceedings of the National Academy of Sciences. 2005;102(43):15545-50.
36. Aliee H, Massip F, Qi C, Stella de Biase M, van Nijnatten JL, Kersten ETG, et al. Determinants

of SARS-CoV-2 receptor gene expression in upper and lower airways. medRxiv. 2020.
37. Sikkema L, Strobl D, Zappia L, Madissoon E, Markov N, Zaragosi L, et al. An integrated cell atlas of the human lung in health and disease. bioRxiv. 2022:2022.03.10.483747.
38. Newman AM, Liu CL, Green MR, Gentles AJ, Feng W, Xu Y, et al. Robust enumeration of cell subsets from tissue expression profiles. Nat Methods. 2015;12(5):453-7.
39. Mulay A, Konda B, Garcia G, Jr., Yao C, Beil S, Villalba JM, et al. SARS-CoV-2 infection of primary human lung epithelium for COVID-19 modeling and drug discovery. Cell reports. 2021;35(5):109055-.
40. Salgado-Benvindo C, Thaler M, Tas A, Ogando NS, Bredenbeek PJ, Ninaber DK, et al. Suramin Inhibits SARS-CoV-2 Infection in Cell Culture by Interfering with Early Steps of the Replication Cycle. Antimicrob Agents Chemother. 2020;64(8).
41. Katsura H, Sontake V, Tata A, Kobayashi Y, Edwards CE, Heaton BE, et al. Human Lung Stem Cell-Based Alveolospheres Provide Insights into SARS-CoV-2-Mediated Interferon Responses and Pneumocyte Dysfunction. Cell Stem Cell. 2020;27(6):890-904.e8.
42. Huang J, Hume AJ, Abo KM, Werder RB, Villacorta-Martin C, Alysandratos KD, et al. SARS-CoV-2 Infection of Pluripotent Stem Cell-Derived Human Lung Alveolar Type 2 Cells Elicits a Rapid Epithelial-Intrinsic Inflammatory Response. Cell Stem Cell. 2020;27(6):962-73.e7.
43. Lukassen S, Chua RL, Trefzer T, Kahn NC, Schneider MA, Muley T, et al. SARS-CoV-2 receptor ACE2 and TMPRSS2 are primarily expressed in bronchial transient secretory cells. EMBO J. 2020;39(10):e105114-e.
44. Amatngalim GD, Schrumpf JA, Dishchekenian F, Mertens TCJ, Ninaber DK, van der Linden AC, et al. Aberrant epithelial differentiation by cigarette smoke dysregulates respiratory host defence. Eur Respir J. 2018;51(4).
45. Mertens TCJ, van der Does AM, Kistemaker LE, Ninaber DK, Taube C, Hiemstra PS. Cigarette smoke differentially affects IL-13-induced gene expression in human airway epithelial cells. Physiological reports. 2017;5(13).
46. Zhang H, Rostami MR, Leopold PL, Mezey JG, O'Beirne SL, Strulovici-Barel Y, et al. Expression of the SARS-CoV-2 ACE2 Receptor in the Human Airway Epithelium. American journal of respiratory and critical care medicine. 2020;202(2):219-29.
47. Lieberman NAP, Peddu V, Xie H, Shrestha L, Huang M-L, Mears MC, et al. In vivo antiviral host transcriptional response to SARS-CoV-2 by viral load, sex, and age. PLOS Biology. 2020;18(9):e3000849.
48. Vanderheiden A, Ralfs P, Chirkova T, Upadhyay AA, Zimmerman MG, Bedoya S, et al. Type I and Type III Interferons Restrict SARS-CoV-2 Infection of Human Airway Epithelial Cultures. 2020;94(19):e00985-20.
49. Liao Y, Li X, Mou T, Zhou X, Li D, Wang L, et al. Distinct infection process of SARS-CoV-2 in human bronchial epithelial cell lines. J Med Virol. 2020;92(11):2830-8.
50. Ziegler CGK, Allon SJ, Nyquist SK, Mbano IM, Miao VN, Tzouanas CN, et al. SARS-CoV-2 Receptor ACE2 Is an Interferon-Stimulated Gene in Human Airway Epithelial Cells and Is Detected in Specific Cell Subsets across Tissues. Cell. 2020;181(5):1016-35.e19.
51. Bost P, Giladi A, Liu Y, Bendjelal Y, Xu G, David E, et al. Host-Viral Infection Maps Reveal Signatures of Severe COVID-19 Patients. Cell. 2020;181(7):1475-88.e12.
52. Ruiz García S, Deprez M, Lebrigand K, Cavard A, Paquet A, Arguel MJ, et al. Novel dynamics of human mucociliary differentiation revealed by single-cell RNA sequencing of nasal epithelial cultures. Development. 2019;146(20).
53. Vieira Braga FA, Kar G, Berg M, Carpaij OA, Polanski K, Simon LM, et al. A cellular census

of human lungs identifies novel cell states in health and in asthma. Nature Medicine. 2019;25(7):1153-63.

54. Kimura H, Francisco D, Conway M, Martinez FD, Vercelli D, Polverino F, et al. Type 2 inflammation modulates ACE2 and TMPRSS2 in airway epithelial cells. J Allergy Clin Immunol. 2020;146(1):80-8.e8.
55. Eger K, Bel EH. Asthma and COVID-19: do we finally have answers? Eur Respir J. 2021;57(3).
56. Morrison CB, Edwards CE, Shaffer KM, Araba KC, Wykoff JA, Williams DR, et al. SARS-CoV-2 infection of airway cells causes intense viral and cell shedding, two spreading mechanisms affected by IL-13. Proceedings of the National Academy of Sciences of the United States of America. 2022;119(16):e2119680119.
57. Bonser LR, Eckalbar WL, Rodriguez L, Shen J, Koh KD, Ghias K, et al. The Type 2 Asthma Mediator IL-13 Inhibits Severe Acute Respiratory Syndrome Coronavirus 2 Infection of Bronchial Epithelium. 2022;66(4):391-401.
58. Liu Y, Lv J, Liu J, Li M, Xie J, Lv Q, et al. Mucus production stimulated by IFN-AhR signaling triggers hypoxia of COVID-19. Cell Res. 2020;30(12):1078-87.
59. Ravindra NG, Alfajaro MM, Gasque V, Huston NC, Wan H, Szigeti-Buck K, et al. Single-cell longitudinal analysis of SARS-CoV-2 infection in human airway epithelium identifies target cells, alterations in gene expression, and cell state changes. PLoS Biol. 2021;19(3):e3001143.
60. Zhao M-M, Yang W-L, Yang F-Y, Zhang L, Huang W-J, Hou W, et al. Cathepsin L plays a key role in SARS-CoV-2 infection in humans and humanized mice and is a promising target for new drug development. Signal Transduction and Targeted Therapy. 2021;6(1):134.
61. Wang Y, Thaler M, Ninaber DK, van der Does AM, Ogando NS, Beckert H, et al. Impact of human airway epithelial cellular composition on SARS-CoV-2 infection biology. bioRxiv. 2021:2021.07.21.453304.

Supplementary figures

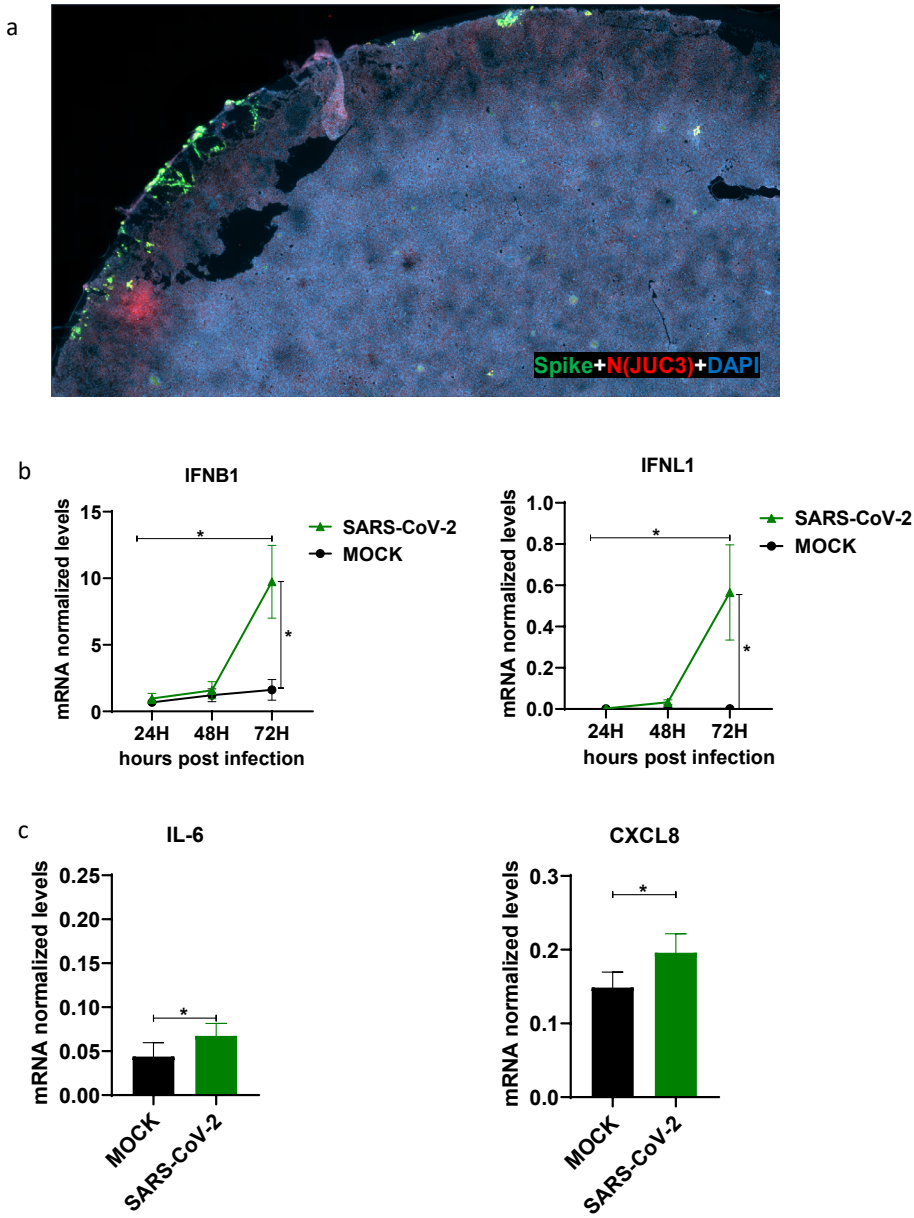

Supplementary Figure 1. Infection and immune responses of a primary airway epithelial cell culture model. ALI-PBEC (mix of 5 donors) cultured for 5 weeks at ALI were infected with SARS-CoV-2 (30,000 PFU per insert) (a) Representative image of immunostaining with anti-SARS-CoV-2 spike protein antibody (green), anti-N protein antibody (JUC3; red) and DAPI (blue) for nuclear staining was captured by ZEISS slide scanner (b) Analysis of gene expression of *IFNB1*, *IFNL1* and (c) *IL6* and *CXCL8* normalized to two reference genes (*RPL13A/ATP5B*) in mixes of 5 donors by RT-qPCR. The graphs

represent the mRNA levels at 72 hpi. Data are mean values ± SEM. n=3 independent experiments derived from the same donor mix cultured for at least 4 weeks. Statistical analysis was conducted using two-way ANOVA with a Tukey/Bonferroni post-hoc test or paired nonparametric t test followed with Wilcoxon matched-pairs signed rank test. Significant differences are indicated by *P<0.05.

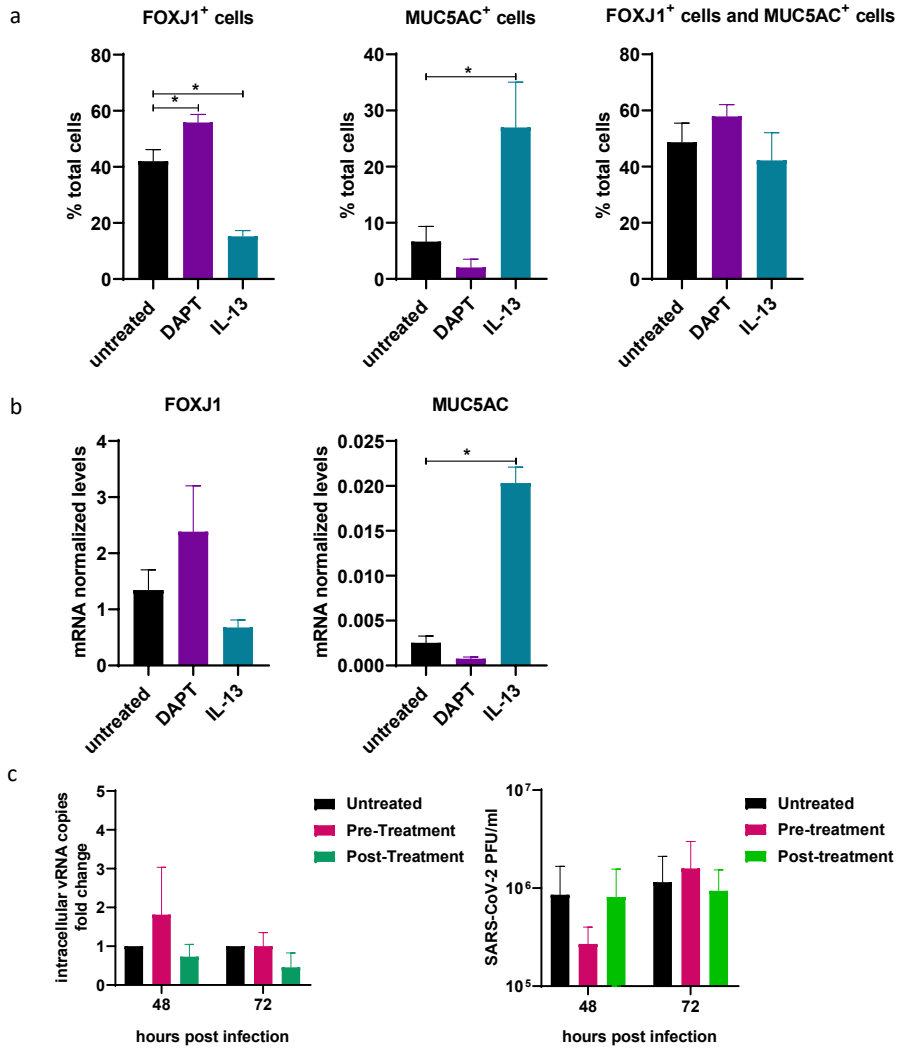

Supplementary Figure 2. Effect of long-term DAPT/IL-13 exposure on epithelial cell composition and effect of acute DAPT/IL-13 exposure on susceptibility to SARS-CoV-2 infection. ALI-PBEC (mix of 4-5 donors) were differentiated for 3 weeks, before addition of DAPT (5 µM) or IL-13 (1 ng/ml), followed by differentiation for an additional 2 weeks. (a) After 5 weeks of differentiation, ALI-PBEC were fixed, stained and analyzed by immunofluorescence using primary antibodies against MUC5AC and FOXJ1 (goblet cell marker, ciliated cell marker) in combination with DAPI for nuclear staining. The quantification of FOXJ1-positive cells and MUC5AC-positive cells was done by ImageJ software.

Data are mean ± SEM. (b) mRNA levels of *FOXJ1* and *MUC5AC* were measured by RT-qPCR. Data are mean ± SEM. Analysis of differences was conducted using paired t test. (c) Short-term treatment with DAPT was performed in cells after 5 weeks of differentiation. Cells were either pre-treated with DAPT for 24 h (pre-treatment) or post-treated directly after infection (post-treatment). Intracellular SARS-CoV-2 RNA copies were measured by RT-qPCR and plaque assay was performed with apical washes to quantify infectious virus titers. n=3 independent experiments. Data are mean ± SEM. Fold change in intracellular RNA copies was compared to untreated controls. Statistical analysis was performed using a paired t test. Significant differences are indicated by *P<0.05.

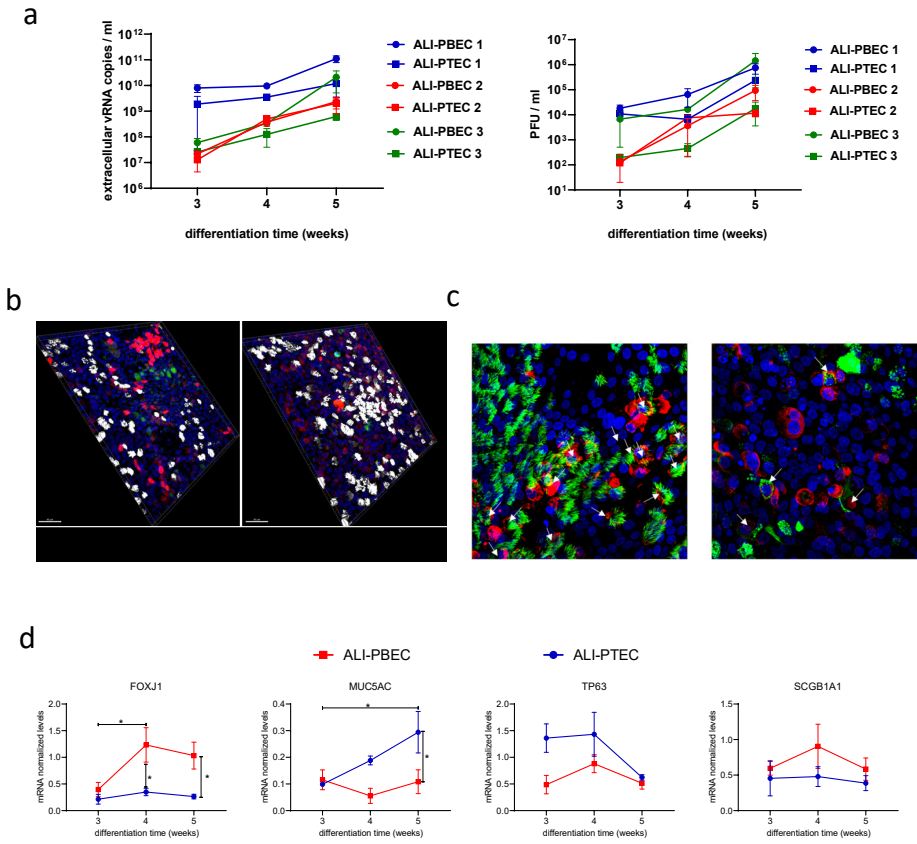

Supplementary Figure 3. Effect of culture duration on infection and epithelial cell-specific genes in PTEC and PBEC. (a) Extracellular viral RNA copies in the apical wash were measured by RT-qPCR and viral infectious progeny was determined by plaque assay in Vero E6 cells. Mean values ± SEM is presented from 3 independent experiments using 3 different donor mixes. (b) Immunofluorescence staining of PTEC and PBEC with antibodies against CC-10 (Club cell marker), MUC5AC (goblet cell marker), acetylated α-tubulin (ciliated cell marker) in combination with DAPI for nuclear staining. (c) Immunofluorescence staining of PTEC with antibodies against acetylated α-tubulin and SARS-CoV-2 N protein in combination with DAPI. Immunofluorescence images shown are representative for results of 3 independent experiments with 630 x original magnification. (d) ALI-PTEC/PBEC (mix of 5 donors) were differentiated at ALI for 3, 4 or 5 weeks, and analyzed by RT-qPCR to measure gene expression of

FOXJ1 (ciliated cell marker), MUC5AC (goblet cell marker), SCGB1A1 (club cell marker) and TP63 (basal cell marker). n=3 independent experiments at 3-5 weeks derived from three donor mixes the same as used in Fig.3. Data are mean ± SEM. Analysis of differences was conducted using two-way ANOVA with a Tukey/Bonferroni post-hoc test. Significant differences are indicated by *P<0.05.

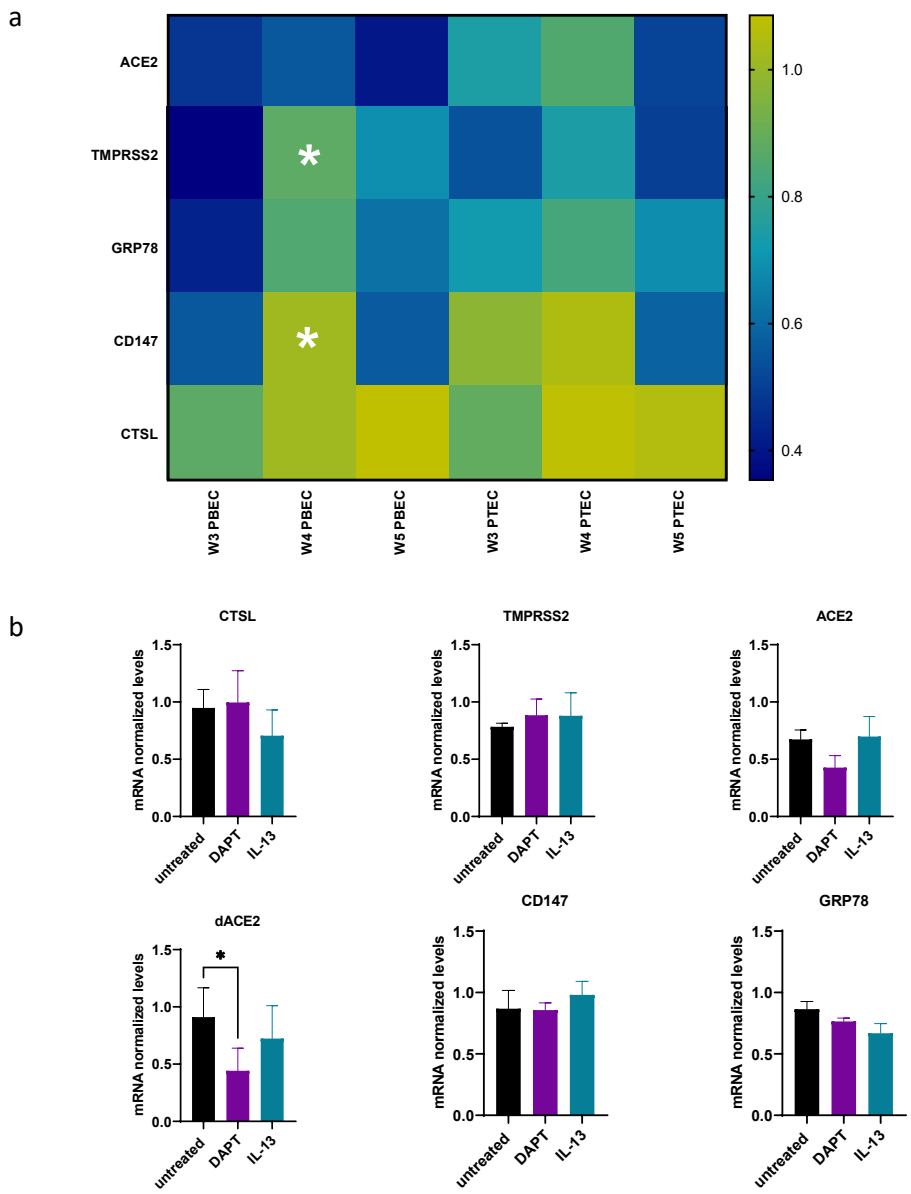

Supplementary Figure 4. Effect of culture duration and DAPT/IL13 treatment on expression of SARS-CoV-2 cell-entry factors. (a) Analysis of gene expression of viral cell-entry factors by RT-qPCR in 3, 4 and 5 week uninfected cultures of PTEC and PBEC and (b) in DAPT or IL-13 treated 5 week-

differentiated cultures. Data are mean values ± SEM. n=3 independent experiments derived from three donor mixes. Statistical analysis was conducted using two-way ANOVA with a Tukey post-hoc test or one-way ANOVA with Dunnett test. Significant differences are indicated by P<0.05. *= 5-week ALI-PBEC vs 3-week ALI-PBEC.

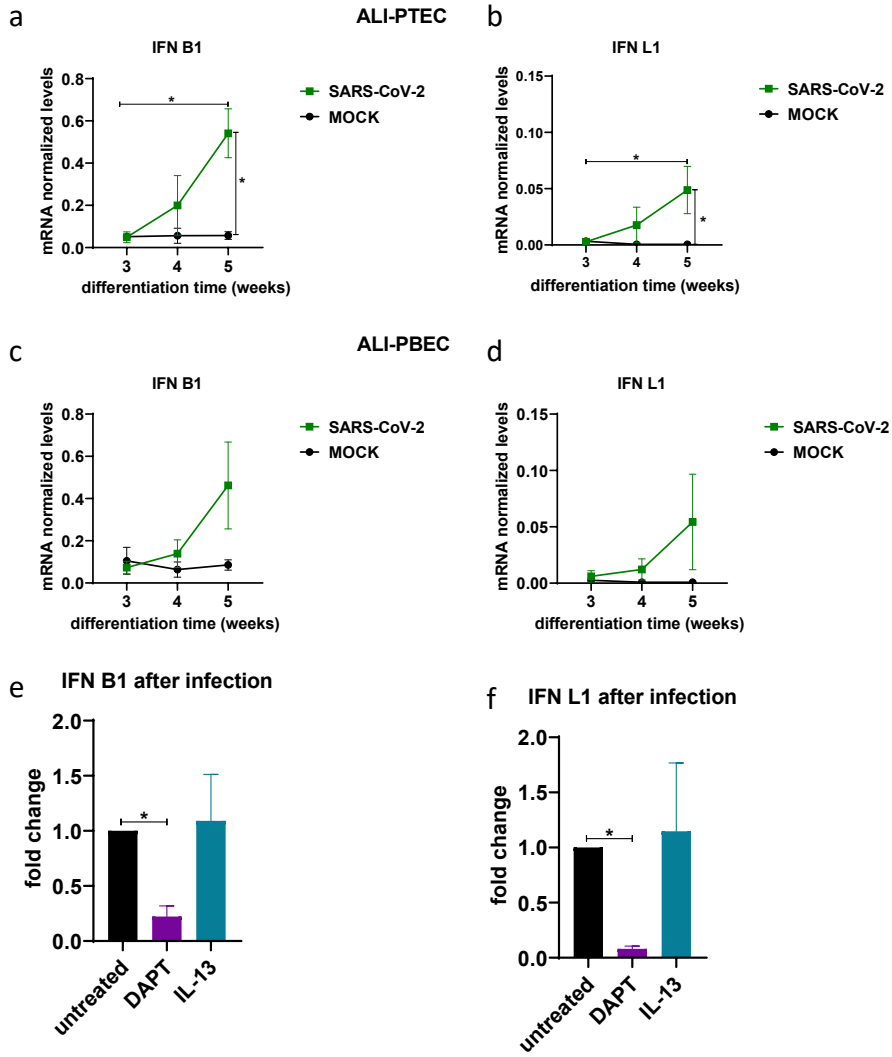

Supplementary Figure 5. Antiviral responses after SARS-CoV-2 infection. ALI-PTEC and PBEC cultured for 3-5 weeks, and 5-week ALI-PBEC cultured at ALI in presence or absence of DAPT or IL-13 (during the last 2 weeks), were infected by SARS-CoV-2 (30,000 PFU per insert). Cells were lysed at 72 hpi to quantify mRNA levels of IFNB1 (a/c/e) and IFNL1 (b/d/f) by RT-qPCR. n=3 independent experiments using 3 different donor mixes. Data are mean ± SEM. Fold change in E and F was compared to untreated controls. Analysis of differences was conducted using two-way ANOVA with a Tukey/Bonferroni post-hoc test. Significant differences are indicated by *P<0.05.

Table S1. The differentially expressed genes in ALI-PBEC and ALI-PTEC between 3-week and 5-week cultures

Gene symbol	logFC	logCPM	F	P value	FDR
ALI-PBEC					
GBP1	1,003	5,593	28,427	0,000	0,012
C6	1,009	4,599	34,176	9,24E-5	0,011
FAM13C	1,015	1,687	15,427	0,002	0,029
NMNAT2	1,040	2,464	27,226	0,000	0,013
VEPH1	1,041	1,216	12,345	0,005	0,041
KIF26B	1,047	2,465	23,288	0,000	0,015
SUSD5	1,049	0,594	13,237	0,004	0,038
ALS2CR12	1,053	3,056	27,673	0,000	0,012
TEKT3	1,073	0,718	21,286	0,001	0,017
ADH7	1,076	6,748	33,320	0,000	0,011
SLC1A1	1,077	5,080	21,270	0,001	0,017
GCNT4	1,079	1,613	23,971	0,000	0,014
GNA14	1,082	2,956	12,760	0,004	0,039
SERPING1	1,084	3,389	23,873	0,000	0,014
CXCL3	1,088	3,836	9,254	0,011	0,065
LINC00689	1,102	1,213	7,918	0,016	0,081
RP11-356I2.4	1,123	0,167	18,212	0,001	0,022
CCL20	1,124	4,278	10,844	0,007	0,051
CCDC173	1,129	4,662	32,157	0,000	0,011
SFRP2	1,130	1,309	10,195	0,008	0,056
ARG2	1,131	2,939	13,980	0,003	0,035
GLYATL2	1,139	0,779	13,648	0,003	0,036
ZNF853	1,145	0,872	7,059	0,022	0,096
ACTBL2	1,146	1,203	14,673	0,003	0,031
OXGR1	1,154	0,362	8,222	0,015	0,077
TM6SF1	1,158	0,157	15,950	0,002	0,027
ZSCAN12P1	1,177	0,305	10,770	0,007	0,052
AFAP1L2	1,185	2,239	12,236	0,005	0,042
UCHL1	1,187	1,026	11,456	0,006	0,047
UCA1	1,203	2,242	8,054	0,015	0,080
DMBT1	1,214	5,708	29,854	0,000	0,011
CES1	1,221	5,122	37,278	6,28E-5	0,011
SLC5A1	1,232	3,193	47,331	2,09E-5	0,008
RP11-642P15.1	1,259	0,950	23,233	0,000	0,015

EEF1A2	1,292	1,560	6,937	0,022	0,098
RP1-27K12.2	1,303	2,755	16,993	0,002	0,024
IL22RA1	1,313	0,206	11,123	0,006	0,049
HLA-DQA1	1,318	3,114	9,050	0,011	0,067
CYP24A1	1,331	3,752	8,917	0,012	0,069
RGS22	1,388	3,305	31,341	0,000	0,011
SLC6A20	1,428	2,040	23,023	0,000	0,015
MAP1B	1,431	3,969	17,918	0,001	0,023
CTSV	1,492	3,622	16,421	0,002	0,026
NCR3LG1	1,550	1,735	35,598	7,72E-5	0,011
CXCL5	1,558	3,177	9,935	0,009	0,058
CHI3L1	1,577	1,837	20,733	0,001	0,018
GPNMB	1,700	6,046	14,867	0,002	0,031
AL121901.1	1,810	1,657	10,005	0,009	0,058
SLC5A8	1,837	1,719	17,359	0,001	0,024
SPTBN4	-2,091	2,377	25,715	0,000	0,014
AC022596.6	-2,053	2,060	15,327	0,002	0,029
EXOC3L1	-1,824	1,024	14,227	0,003	0,034
PLCD4	-1,768	1,754	22,924	0,000	0,015
IQGAP3	-1,745	0,909	11,256	0,006	0,048
LGALS7	-1,709	4,388	19,047	0,001	0,021
LGALS7B	-1,692	3,764	26,461	0,000	0,013
CYP26C1	-1,648	1,059	15,954	0,002	0,027
CYP4F23P	-1,646	2,029	12,522	0,004	0,040
ASPM	-1,638	1,458	11,777	0,005	0,045
PLA2G4F	-1,636	2,389	11,336	0,006	0,047
PDE11A	-1,609	3,469	10,129	0,008	0,057
MAOB	-1,572	1,720	19,532	0,001	0,020
KRT13	-1,571	8,159	17,332	0,001	0,024
WNT10A	-1,557	5,014	88,117	9,64E-7	0,003
KLK7	-1,529	4,872	17,553	0,001	0,023
MYOT	-1,492	1,384	12,493	0,004	0,041
ALOX15B	-1,424	4,068	30,081	0,000	0,011
CKAP2L	-1,424	0,388	7,750	0,017	0,084
KCNE4	-1,404	1,776	12,700	0,004	0,040
KLK8	-1,390	1,395	27,354	0,000	0,013
EFS	-1,325	1,431	16,957	0,002	0,024
COL7A1	-1,296	7,750	40,824	4,15E-5	0,009
MEGF6	-1,280	4,889	28,198	0,000	0,012

CYP26B1	-1,279	7,617	9,466	0,010	0,063
PLCH2	-1,275	6,836	48,420	1,87E-5	0,008
RP5-1085F17.3	-1,266	0,327	18,203	0,001	0,022
TNNI2	-1,261	4,254	11,143	0,006	0,049
RP11-235E17.6	-1,260	2,578	19,506	0,001	0,020
FGFR3	-1,259	7,297	110,697	2,94E-7	0,002
EGFL6	-1,245	3,666	12,448	0,004	0,041
HMHA1	-1,244	3,559	7,979	0,016	0,080
MMP28	-1,243	5,290	45,789	2,44E-5	0,008
GPT	-1,239	0,373	12,289	0,005	0,042
CLEC2D	-1,238	1,919	19,119	0,001	0,020
RHBDL1	-1,237	2,114	19,162	0,001	0,020
ECM1	-1,229	4,151	12,244	0,005	0,042
MEX3B	-1,221	1,358	8,708	0,013	0,071
RP11-268J15.5	-1,209	2,564	22,611	0,001	0,015
CYP2T2P	-1,208	6,447	21,978	0,001	0,016
FAM229A	-1,206	2,869	20,508	0,001	0,018
CSRNP3	-1,201	1,440	11,400	0,006	0,047
PCP2	-1,201	0,595	7,174	0,021	0,093
PLK1	-1,198	1,866	17,228	0,001	0,024
CAPNS2	-1,194	1,982	11,370	0,006	0,047
ADIRF	-1,190	3,254	34,076	9,36E-5	0,011
PTTG1	-1,189	3,122	32,071	0,000	0,011
BDKRB1	-1,175	0,394	17,478	0,001	0,023
GHR	-1,172	0,534	9,381	0,010	0,064
ANKRD9	-1,164	4,306	25,466	0,000	0,014
FOXN4	-1,163	3,313	11,793	0,005	0,045
HSD11B2	-1,158	4,532	14,920	0,002	0,030
IGFBP6	-1,154	7,240	108,504	3,27E-7	0,002
KRT14	-1,149	4,979	10,559	0,007	0,053
RP11-44N21.1	-1,149	0,745	11,824	0,005	0,044
VMO1	-1,148	7,731	34,330	9,06E-5	0,011
NAPSA	-1,145	0,737	9,183	0,011	0,066
KCP	-1,143	2,294	29,445	0,000	0,012
WFDC3	-1,143	2,557	10,057	0,008	0,057
CENPE	-1,142	1,281	7,721	0,017	0,084
CFD	-1,140	3,218	14,735	0,003	0,031
TMEM160	-1,139	3,550	30,432	0,000	0,011
SNCG	-1,138	2,811	21,100	0,001	0,017

AIFM3	-1,136	2,051	11,133	0,006	0,049
RBBP8NL	-1,134	3,471	18,302	0,001	0,022
CTU1	-1,130	2,728	17,317	0,001	0,024
ABCC9	-1,129	4,377	24,044	0,000	0,014
KLK6	-1,127	3,031	9,410	0,010	0,064
RP11-108K14.4	-1,124	3,404	47,919	1,97E-5	0,008
FES	-1,121	2,078	17,204	0,001	0,024
HSPB1	-1,118	8,552	77,271	1,89E-6	0,004
PRSS3	-1,116	1,316	9,743	0,009	0,060
CHRM3	-1,112	2,126	11,384	0,006	0,047
POU5F1	-1,111	3,686	8,313	0,014	0,076
CDCA3	-1,105	0,746	9,323	0,010	0,064
LIME1	-1,105	2,078	16,872	0,002	0,025
UNC5CL	-1,101	1,165	9,879	0,009	0,059
RP11-538D16.2	-1,100	1,293	10,810	0,007	0,051
AC009061.1	-1,096	2,198	15,632	0,002	0,028
NDUFA13	-1,089	1,375	11,114	0,006	0,049
UCN2	-1,085	1,380	17,168	0,001	0,024
GPS2	-1,084	1,109	8,343	0,014	0,076
ANKRD2	-1,081	0,647	7,805	0,017	0,083
CYP2E1	-1,078	2,402	19,559	0,001	0,020
HES6	-1,074	4,396	24,817	0,000	0,014
RP5-1074L1.4	-1,074	1,133	8,676	0,013	0,072
HCN3	-1,072	2,946	33,765	9,75E-5	0,011
NYAP1	-1,068	-0,307	8,367	0,014	0,075
ADAMTSL4	-1,068	4,669	8,592	0,013	0,073
C19orf40	-1,065	0,538	9,758	0,009	0,060
LTBP4	-1,065	6,480	36,662	6,76E-5	0,011
KIFC1	-1,062	0,993	7,845	0,017	0,082
ADAMTSL5	-1,052	3,978	18,222	0,001	0,022
FAM173A	-1,049	3,761	38,476	5,44E-5	0,010
C12orf54	-1,046	0,473	8,517	0,013	0,074
AP001053.11	-1,045	1,784	18,498	0,001	0,022
WNT2B	-1,042	1,990	16,133	0,002	0,026
KDR	-1,040	3,401	12,145	0,005	0,043
IQCJ-SCHIP1	-1,037	0,963	14,415	0,003	0,033
NFATC4	-1,036	5,419	22,169	0,001	0,016
PRKCDBP	-1,035	4,922	34,123	9,31E-5	0,011
PRICKLE4	-1,035	6,186	30,469	0,000	0,011

SPINK5	-1,034	4,561	11,508	0,006	0,046
DLK2	-1,034	3,666	33,642	9,91E-5	0,011
PLEKHH3	-1,033	6,091	109,429	3,12E-7	0,002
PPP1R35	-1,033	3,718	16,700	0,002	0,025
FLG-AS1	-1,028	3,841	15,164	0,002	0,030
BRICD5	-1,023	2,700	13,735	0,003	0,036
TNFRSF25	-1,020	4,588	44,426	2,81E-5	0,009
TRIM7	-1,018	3,732	39,009	5,11E-5	0,010
PTMS	-1,018	6,405	33,334	0,000	0,011
RP11-783K16.13	-1,014	1,096	13,996	0,003	0,034
CTD-3214H19.6	-1,013	0,205	7,515	0,018	0,087
PCDHB15	-1,013	1,237	16,920	0,002	0,024
RP11-258C19.7	-1,012	1,281	11,744	0,005	0,045
PHYHIP	-1,011	4,107	36,227	7,14E-5	0,011
AC005262.2	-1,007	1,245	8,153	0,015	0,078
ZNF648	-1,006	3,003	13,408	0,003	0,037
DBP	-1,005	4,434	24,402	0,000	0,014
GDPD3	-1,000	2,191	19,863	0,001	0,020

ALI-PTEC					
DMBT1	1,004	5,708	20,072	0,001	0,077
ANKFN1	1,036	3,177	26,042	0,000	0,068
RP11-247L20.4	1,039	0,904	17,573	0,001	0,085
CCDC173	1,040	4,662	24,830	0,000	0,068
NCR3LG1	1,076	1,735	14,666	0,003	0,091
VNN3	1,103	2,740	20,957	0,001	0,075
PTPRT	1,122	3,408	44,670	2,74E-5	0,053
AC005281.1	1,152	1,905	15,931	0,002	0,089
FAM167A	1,161	1,696	18,336	0,001	0,081
DSCAML1	1,161	1,539	18,199	0,001	0,082
PLA1A	1,166	1,233	17,360	0,001	0,085
RND2	1,189	2,016	16,128	0,002	0,089
SUSD5	1,196	0,594	16,288	0,002	0,089
DAAM2	1,200	1,531	15,378	0,002	0,090
COL28A1	1,232	3,080	27,896	0,000	0,062
USH1C	1,286	1,141	19,777	0,001	0,077
TMEM176B	1,310	2,703	25,333	0,000	0,068
CES1	1,319	5,122	39,111	5,05E-5	0,053
VEPH1	1,331	1,216	14,554	0,003	0,092

RGS22	1,340	3,305	26,620	0,000	0,065
CXCL6	1,348	4,337	29,333	0,000	0,062
CCL20	1,381	4,278	16,829	0,002	0,088
RP11-642P15.1	1,388	0,950	18,688	0,001	0,080
TMEM176A	1,425	2,425	39,546	4,80E-5	0,053
TCHH	1,430	2,342	21,012	0,001	0,075
MACROD2	1,458	1,357	23,452	0,000	0,068
BDNF	1,499	0,728	14,385	0,003	0,092
GRM7	1,535	2,011	35,114	8,20E-5	0,053
CYP2A13	1,644	4,777	14,510	0,003	0,092
CHI3L1	1,646	1,837	24,199	0,000	0,068
CXCL5	2,160	3,177	19,961	0,001	0,077
SLC5A8	2,199	1,719	23,757	0,000	0,068
IQGAP3	-2,593	0,909	22,710	0,001	0,068
ASPM	-1,891	1,458	15,385	0,002	0,090
KLK7	-1,837	4,872	25,617	0,000	0,068
CENPE	-1,787	1,281	17,972	0,001	0,082
FBXO24	-1,419	0,140	16,181	0,002	0,089
ARHGAP11B	-1,392	1,101	25,090	0,000	0,068
PLCD4	-1,370	1,754	14,044	0,003	0,097
MAOB	-1,321	1,720	16,321	0,002	0,089
ECM1	-1,320	4,151	15,937	0,002	0,089
LGALS7B	-1,276	3,764	16,058	0,002	0,089
UCN2	-1,270	1,380	24,582	0,000	0,068
LMNB1	-1,234	2,203	15,192	0,002	0,091
KRT14	-1,232	4,979	15,695	0,002	0,090
GPR37L1	-1,194	2,348	29,309	0,000	0,062
MAP2	-1,190	2,347	23,380	0,000	0,068
TENM2	-1,163	2,101	21,716	0,001	0,070
RP4-758J18.10	-1,145	0,954	14,161	0,003	0,095
NXPH4	-1,126	2,060	20,226	0,001	0,077
RHBDL1	-1,112	2,114	15,530	0,002	0,090
SEMA6A	-1,112	2,970	21,650	0,001	0,070
ALDOC	-1,102	4,806	15,560	0,002	0,090
ALOX15B	-1,099	4,068	20,082	0,001	0,077
CA9	-1,047	3,850	37,164	6,36E-5	0,053
FIBIN	-1,037	1,318	15,218	0,002	0,091
CLDN8	-1,011	4,270	18,618	0,001	0,080
WNT10A	-1,011	5,014	39,609	4,77E-5	0,053